

# Seismic velocity analysis using spectral bandwidth

Bachelor Thesis of Ben Schmidt

**Institute of Geophysics  
University of Hamburg  
Hamburg, Germany**

July 2019

Topic: Automatic velocity analysis using spectral bandwidth

# 1 Abstract

To get a good image of the subsurface it is crucial to know the seismic velocities to convert the measured travel times into depths. In this Bachelor Thesis I try to figure out a better way than the semblance to get the normal-moveout-velocities  $v_{\text{NMO}}$  for a common-midpoint-gather by using the bandwidth of the stacked traces.

For this I created two synthetic CMP-gathers, one with noise and one without noise, containing a single reflection of a ricker wavelet. Moreover I used a CMP from a data set recorded in the Mediterranean sea.

When reflections, that were NMO-corrected with a wrong velocity, are stacked the resulting signals get longer in the time domain. As a consequence of Heisenberg's uncertainty principle their spectral bandwidth is therefore reduced.

However, it is not possible to use the conventional definition of bandwidth and ignore the amplitudes of the stacked signals. This method only works if the bandwidth is defined relative to a reference spectrum that contains information about the amplitude. In this case for every time window I used the power spectrum with the highest maximum as a reference spectrum.

When multiple signals occur simultaneously the bandwidth method delivers normal-moveout-velocities more precisely than the semblance. Otherwise both methods deliver similar results.

A disadvantage is that it takes more computational effort and implementing an automated velocity picking would be more difficult than with the semblance method.



# Contents

<b>1</b>	<b>Abstract</b>	<b>3</b>
<b>2</b>	<b>Introduction</b>	<b>6</b>
<b>3</b>	<b>Theory</b>	<b>7</b>
3.1	Travel time curves . . . . .	7
3.2	Geometrical spreading, reflection coefficient and absorption . . . . .	9
3.3	NMO-correction and NMO-stretch . . . . .	9
3.4	Semblance coefficient and spread length . . . . .	10
3.5	FFT and spectral analysis . . . . .	12
3.6	Heisenberg's uncertainty principle . . . . .	13
3.7	Stacking with wrong velocity . . . . .	13
<b>4</b>	<b>Data sets and processing</b>	<b>17</b>
4.1	Amplitude adaptation, NMO-correction and stacking . . . . .	17
4.2	Semblance and power spectra . . . . .	19
<b>5</b>	<b>Results and discussion</b>	<b>19</b>
5.1	One time window that contains the seafloor reflection . . . . .	19
5.1.1	Semblance . . . . .	23
5.1.2	Conventional definition of bandwidth . . . . .	23
5.1.3	New definition of bandwidth . . . . .	27
5.2	Entire trace length . . . . .	27
<b>6</b>	<b>Quality control</b>	<b>32</b>
6.1	Picked velocities . . . . .	32
6.2	Migrated data . . . . .	36
6.3	Seismic Unix . . . . .	36
<b>7</b>	<b>Conclusions and Outlook</b>	<b>40</b>
<b>8</b>	<b>Acknowledgement</b>	<b>41</b>
<b>9</b>	<b>References</b>	<b>41</b>
<b>10</b>	<b>List of Figures</b>	<b>42</b>
<b>11</b>	<b>Versicherung an Eides statt</b>	<b>43</b>

## 2 Introduction

The objective of applied seismic is to get a model of the subsurface. For this it is necessary to convert the measured two-way travel times into depth. Mostly this is done with depth conversion, for which a good velocity-starting model is crucial to get good results. This starting model can be computed when the normal-moveout-velocities are known. For this the method of semblance was designed. The problem with the semblance is that it often does not focus the correct  $v_{\text{NMO}}$  well, especially at times where multiple reflections are present. This makes it difficult to pick the correct velocity, particularly when automatizing the velocity picking process.

The semblance only uses amplitude information of the stacked trace in relation to the amplitude of all unstacked traces. Using the spectra of the stacked traces we might be able to better locate the correct normal-moveout-velocities. This is why in this Bachelor Thesis I develop an alternative way to get the correct normal-moveout-velocity by using the bandwidth of the stacked traces.

In Chapter 3 I discuss the theory that is needed to understand the data processing and the results of this work. Chapter 4 describes the data sets and the steps of data processing. The main part of this Bachelor Thesis is Chapter 5 in which I develop and discuss the bandwidth method. At the end of Chapter 5 I use Seismic Unix to show that the resulting velocity profile straightens the reflections.

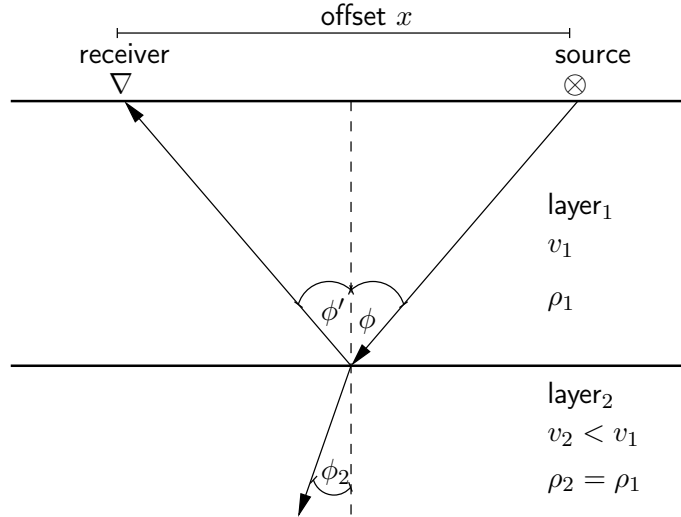


Figure 1: Transmitted and reflected rays in two homogeneous layers with a horizontal layer boundary

### 3 Theory

In these introductory sections I briefly introduce first the main characteristics of seismic waves, namely their travel time and amplitude behavior. This is followed by an explanation of the basic processing steps in applied seismic. Afterwards I explain the semblance method. In the end I describe how to transform signals into the frequency domain and why Heisenberg’s principle can be used to detect whether signals are in phase or not.

Most of this chapter is common knowledge in geophysics and can be looked up in the textbook SEISMIC DATA ANALYSIS by Öz Yilmaz [1]. This is why in this chapter I do not always refer to the original source.

#### 3.1 Travel time curves

In the subsurface seismic waves are partly reflected when the acoustic impedance  $Z = \rho v$  of two layers differ.  $v$  is the propagation-velocity of the wave and  $\rho$  is the density of the medium.

Using a high frequency approximation we can describe seismic waves with rays orthogonal to the wave’s wavefronts. Then we can compute the incident angle of the reflected or transmitted wave with Snell’s Law:

$$\frac{\sin(\phi_i)}{v_i} = \text{const.} \quad . \quad (1)$$

When creating common-midpoint-gathers, also called CMP-gathers, the data is sorted by source-receiver-couples that have the same midpoint. In case of a horizontal reflector all incoming rays are reflected at the same point on the reflector. This is illustrated in Figure 2. The two-way travel time  $t$  of a ray can then be described as a hyperbolic function dependent on the offset  $x$ :

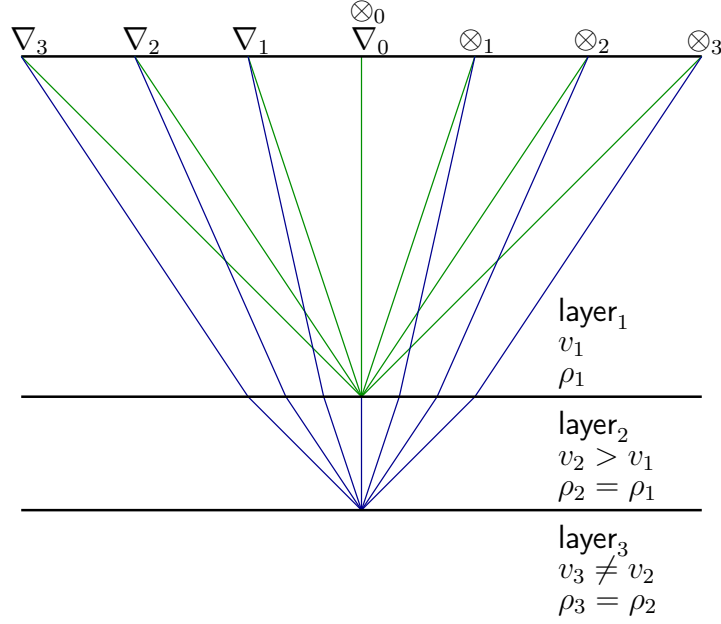


Figure 2: Shot-receiver-couples that belong to a CMP-gather in homogeneous layers with horizontal layer boundaries

$$t = \sqrt{t_0^2 + \frac{x^2}{v_{\text{NMO}}^2}} \quad , \quad (2)$$

with the zero offset time  $t_0 = 2z/v_{\text{NMO}}$ , whereas  $z$  is the depth of the reflector and  $v_{\text{NMO}}$  is the normal-moveout-velocity.

In case of a single horizontal reflector  $v_{\text{NMO}}$  is equal to the propagation-velocity of the wave. When there are multiple horizontal reflectors  $v_{\text{NMO}}$  is equal to  $v_{\text{RMS}}$ , which is the root-of-the-mean-square-velocity. Then it is possible to compute the interval-velocities by using the Dix-inversion [1]:

$$v_{\text{interval},n} = \sqrt{\frac{v_{\text{RMS},n}^2 \cdot t_n - v_{\text{RMS},n-1}^2 \cdot t_{n-1}}{t_n - t_{n-1}}} \quad . \quad (3)$$

Here,  $t_{n-1}$  is the travel time of the wave until it reaches the  $(n-1)$ th reflector,  $t_n$  is the travel time to the  $n$ th reflector and  $v_{\text{RMS}}$  is the root-of-the-mean-square-velocity at the corresponding reflector. Then  $v_{\text{interval},n}$  is the interval-velocity of the layer between the reflector  $n-1$  and  $n$ .

In field data there are many dipping reflectors and there also might be velocity gradients in layers. Therefore the travel time curves are not perfectly hyperbolic and Equation 2 describes the hyperbolic travel time curve that fits the data best. This is why  $v_{\text{NMO}}$  can only be seen as a processing parameter and can not be directly interpreted as a velocity. Nevertheless, if you only expect layer boundaries with small inclinations it can be useful to compute the apparent interval-velocities with the Dix-inversion to check whether picked  $v_{\text{NMO}}$  are realistic or not.

While traveling through the ground the wave's amplitudes changes which would effect the

data processing if it was not taken into account. Therefore the changing amplitudes are discussed in the next introductory section.

### 3.2 Geometrical spreading, reflection coefficient and absorption

In marine seismics the most commonly used source is a water- or airgun. Both are in good approximation an exploding point source. When the wave propagates the wave's energy  $E$  is distributed over a surface  $A$  of increasing size. In a medium with constant seismic velocity this surface is spherical. When  $s$  is the distance that the wave traveled and  $a$  is the amplitude of the wave you get following equations:

$$\frac{1}{E} \propto A \propto s^2 \quad (4)$$

$$a^2 = E \quad (5)$$

$$\Rightarrow a \propto \frac{1}{s} \quad (6)$$

We see that the amplitude of the wave decreases with growing travel distance. When we assume that the wave only propagates in one homogeneous medium and that the reflector is not inclined we get from Equation 2:

$$s = \sqrt{t_0^2 \cdot v_{\text{NMO}}^2 + x^2} \quad (7)$$

Therefore receivers with larger offsets measure smaller amplitudes. In a layered medium with dipping reflectors describing the amplitude decrease due to geometrical spreading is more complicated, but in good approximation we can assume that the wavefront is spherical. The effect of geometrical spreading can then be partly corrected since we have an approximation for the traveled distance from Equation 7. However, the reflected energy also depends on the reflection coefficient, which varies for different incident angles and therefore for different offsets. For correcting this effect we would need a velocity model, which we do not have at that time. Additionally, a part of the energy is absorbed by the material in the ground. This absorption depends on the lithology and on the frequency of the signal. High frequencies are absorbed stronger than low frequencies. Normalizing every trace to its own maximum reduces these effects.

With this knowledge we are able to do the first step in data processing which is explained in the following section.

### 3.3 NMO-correction and NMO-stretch

In an NMO-correction the offset induced part of the travel time is subtracted for every sample in all traces of the CMP-gather:

$$t_{\text{corrected}} = \sqrt{t_{\text{original}}^2 - \frac{x^2}{v_{\text{NMO}}^2}} \quad (8)$$

$T_{\text{original}}$  is the corresponding time of a sample before applying the NMO-correction.  $T_{\text{corrected}}$  is the corresponding time of this sample after applying the NMO-correction. To maintain a constant sample interval it is necessary to interpolate. When the best fitting NMO-velocity is chosen, reflections occur in all traces approximately at the same times. For

different times you will find different velocities that fit best.

A problem is that due to the NMO-correction the length of the signals increases, with the result that the frequency  $f_0$  is reduced by  $\Delta f$ . This is called NMO-stretch [1]. The NMO-stretch can be computed with:

$$\frac{\Delta f}{f_0} = \frac{\Delta t_{\text{NMO}}}{t_0} = \sqrt{1 + \left(\frac{x}{2z}\right)^2} - 1 \quad , \quad (9)$$

$\Delta t_{\text{NMO}} = t - t_0$  is called moveout. The increasing length of the signals due to the NMO-correction is shown in Figure 3.

There is a way to make an NMO-correction without producing an NMO-stretch [2]. The disadvantage of this is that it takes more computational effort, which is why this method is not used in this thesis.

Having applied the NMO-correction the traces can be stacked. This increases the signal-to-noise-ratio by  $\sqrt{n}$ , where  $n$  is the number of traces that are summed up. Because of the NMO-stretch it is recommended to mute traces with high offset-to-target-ratio  $x/z$ . Additionally the approach of hyperbolic travel time curves is only valid for small  $x/z$ . When testing which  $v_{\text{NMO}}$  fits best to straighten the reflections it is very important that the number of muted samples does not change.

Another problem is that we only know the two way time of a reflection and not the reflector depth. If we do not roughly know the seismic velocities in the subsurface we have to guess the velocities to know which samples should be muted. In marine seismics  $v = 1500$  m/s, which is the seismic velocity in water, can be taken:

$$z(t) \approx \frac{t}{2} \cdot 1500 \text{ m/s} \quad . \quad (10)$$

Assuming  $v = 1500$  m/s will probably results in muting too many samples at huge times, because in general the seismic velocity increases with depth. This will result in a slightly worse velocity resolution since we do not have enough moveout at large times.

After having done the velocity analysis it is then possible to do the NMO-correction again, using the determined velocity profile to improve the depth conversion:

$$z(t) \approx \frac{1}{2} \int_0^t v_{\text{interval}}(t') dt' \quad . \quad (11)$$

The differences between these to muting patterns are shown in Figure 24.

Since we do not want to try random velocities by hand to straighten the reflections we need a parameter that delivers suitable stacking velocities. The standard method for this is the semblance which is explained in the following introductory section.

### 3.4 Semblance coefficient and spread length

The semblance  $S$  can be used to automatically determine which  $v_{\text{NMO}}$  fits best. It sets the energy of the stacked trace in relation to the total energy in all unstacked traces:

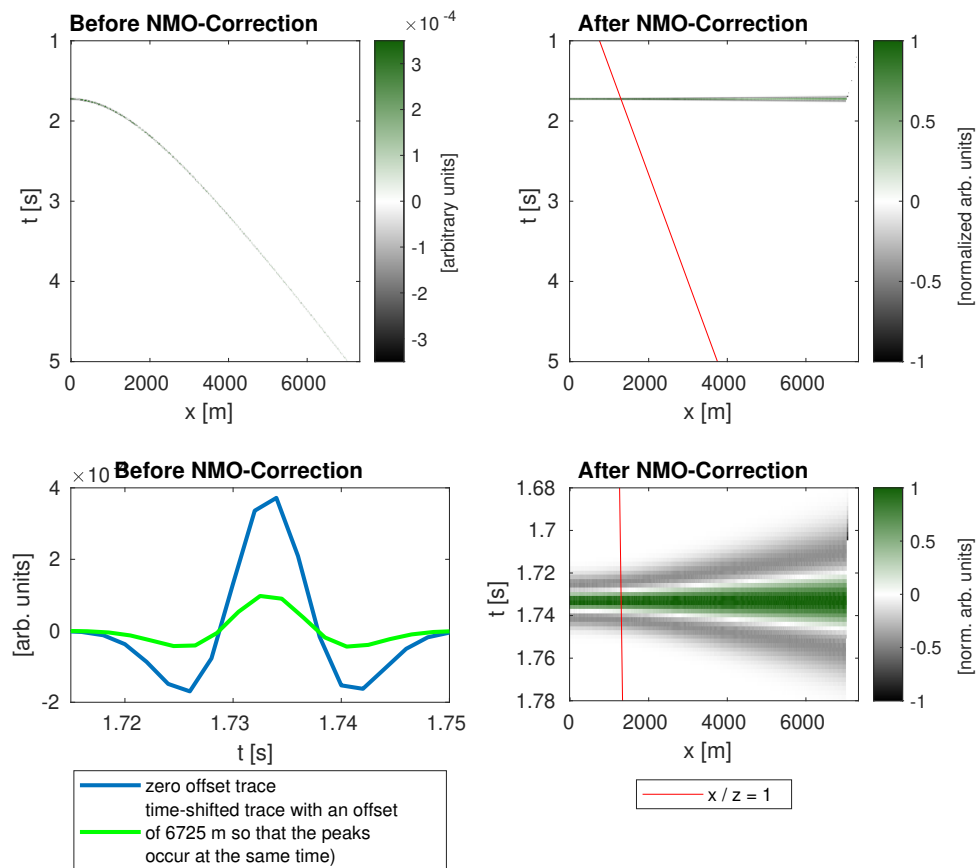


Figure 3: NMO-correction of a synthetic single reflection in a homogeneous layer with a horizontal reflector,  $v=1500$  m/s  
 Top left: CMP-gather before applying the NMO-Correction,  
 Bottom left: Two traces of the CMP-gather before applying the NMO-Correction, the signals have the same length despite the larger offset of the green trace,  
 Top right: CMP-Gather after applying the NMO-Correction,  
 Bottom right: Close-up of the CMP-gather after applying the NMO-Correction

$$S = \frac{\sum_{i=1}^M \left( \sum_{j=1}^N a_{ij} \right)^2}{N \sum_{i=1}^M \sum_{j=1}^N a_{ij}^2} . \quad (12)$$

$M$  is the number of samples in the chosen time window for which the semblance is computed,  $N$  is the number of unmuted traces and  $a_{ij}$  is the  $i$ -th sample of the  $j$ -th trace. Before computing the semblance the traces are normalized to their own maximum in the chosen window. Therefore the semblance can attain values between 0 and 1. Signals that are in phase after the NMO-correction will interfere constructively. A high semblance means that the hyperbolic travel time curve of the chosen  $v_{\text{NMO}}$  fits to the analyzed data.

For a good resolution in velocity moveout is needed and therefore large offset-to-target ratios so that small changes in velocity result in large time-shifts. Because of the problems that were discussed in Section 3.3 it is often useful to choose a maximum  $x/z$  of 1.

Since in this thesis we want to develop an alternative way to find the best fitting velocity using the spectral bandwidth of the signal we need to transform the signal into the frequency domain. The way this can be done is described in the next section.

### 3.5 FFT and spectral analysis

Computing the frequency spectrum of a signal can be done with the Fast-Fourier-Transformation-Function `fft` implemented in `Matlab`, which computes the complex Fourier coefficients  $c_k$  [3]:

$$c_k = \frac{1}{T} \cdot \sum_{n=1}^N x_n \cdot \exp(-i \frac{2\pi}{T} k t_n) . \quad (13)$$

Here  $T$  is the time window length for which the Fourier coefficients are computed and  $N$  is the number of samples in this time window. In our case the analyzed time series are real with the result:

$$c_{-k} = \bar{c}_k \quad (14)$$

$$x(t) = \sum_{k=-N}^N c_k \cdot \exp(i \frac{2\pi}{T} k t) , \quad (15)$$

$c_0$  is the mean value and does not correspond to a frequency. Thus it can be neglected when computing the power spectrum  $P$ . If  $N$  is an odd number the power spectrum and the associated frequencies  $f_k$  can be computed with the following equations [4]:

$$P_{k-1} = \frac{c_k \cdot \bar{c}_k}{N}, k \in [2, \frac{N-1}{2} + 1] \quad (16)$$

$$f_k = \frac{f_{\text{sample}} \cdot k}{N}, k \in [1, \frac{N-1}{2}] . \quad (17)$$

The problem of the FFT is that it only delivers correct results if the signal in the time window can be extended periodically. Otherwise the different values at the margins of the

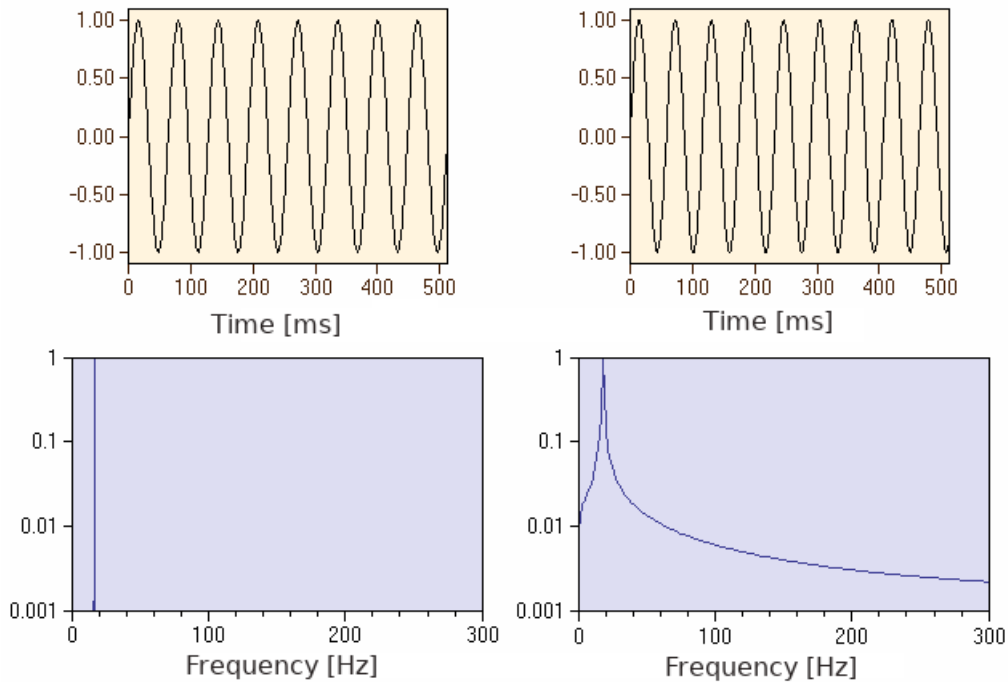


Figure 4: Left: Signal that fits into the time window and can therefore be extended periodically  
 Right: Signal that can not be extended periodically  
 After Hans Lohninger [5], modified by Ben Schmidt

examined interval result in a smeared spectrum. To reduce this effect of the margins it is recommended to multiply the data with a taper window before computing the Fourier coefficients. For a  $\cos^2$ -taper window this is shown in the Figures 4, 5 and 6.

Knowing how to compute power spectra of a signal we can have a closer look on why the bandwidth of a signal might be an indicator for signals that are in phase, but let us first recall Heisenberg's uncertainty principle.

### 3.6 Heisenberg's uncertainty principle

According to Heisenberg's uncertainty principle it is not possible to focus a signal in the time domain and simultaneously in the frequency domain [6]. This means that if the length of a signal increases in the time domain the signal is more focused in the frequency domain.

### 3.7 Stacking with wrong velocity

When stacking traces that were NMO-corrected with a slightly wrong velocity the signals are not in phase. This has several consequences. First of all, the signals become longer in the time domain. This leads to a frequency shift towards lower frequencies and also to a reduction of the spectral bandwidth. Moreover the amplitude of the signal is reduced. This effect is used when applying the semblance method. As a fourth effect further maxima appear in the power spectrum, which make it more difficult to define a bandwidth. The gaps between these maxima are often called notches. All these aspects are shown in

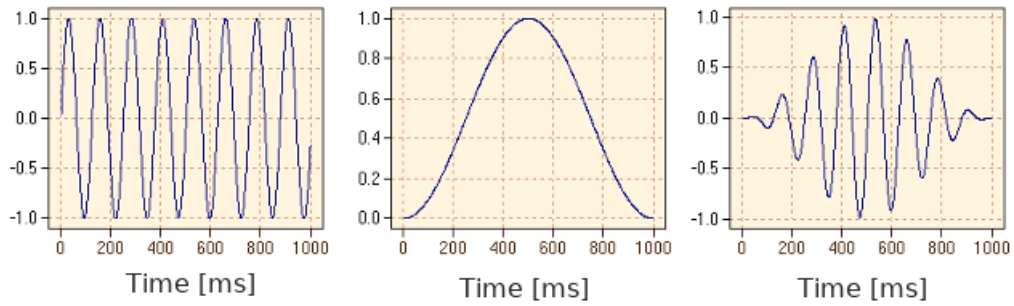


Figure 5: Left: Signal that can not be extended periodically  
 Center:  $\cos^2$  taper window  
 Right: signal multiplied with taper window  
 After Hans Lohninger [5], modified by Ben Schmidt

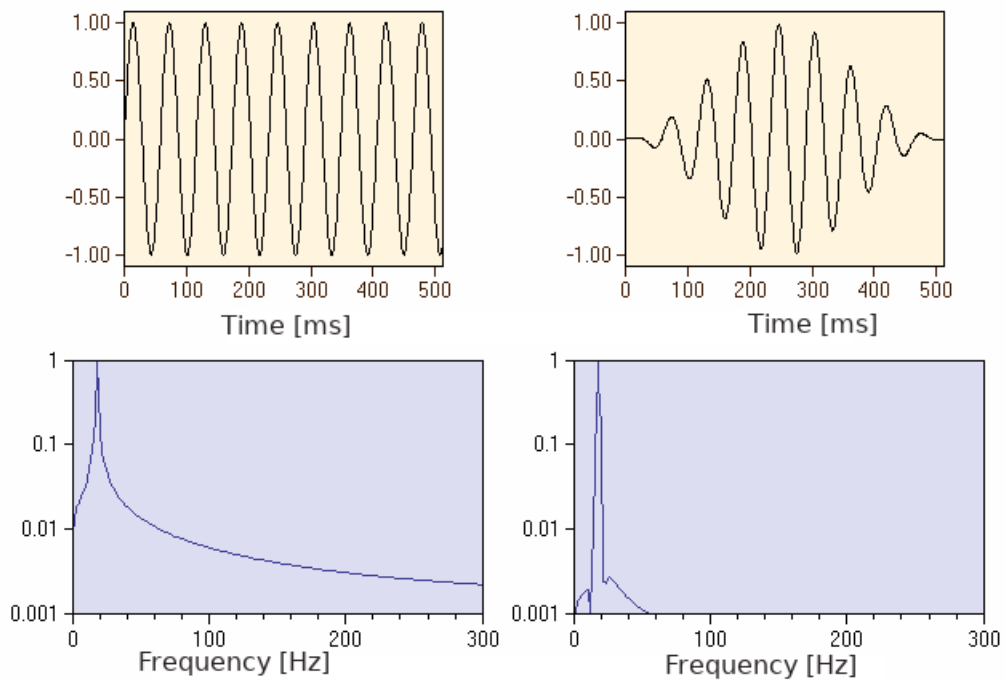


Figure 6: Left: Signal without taper window  
 Right: Signal multiplied with taper window  
 After Hans Lohninger [5], modified by Ben Schmidt

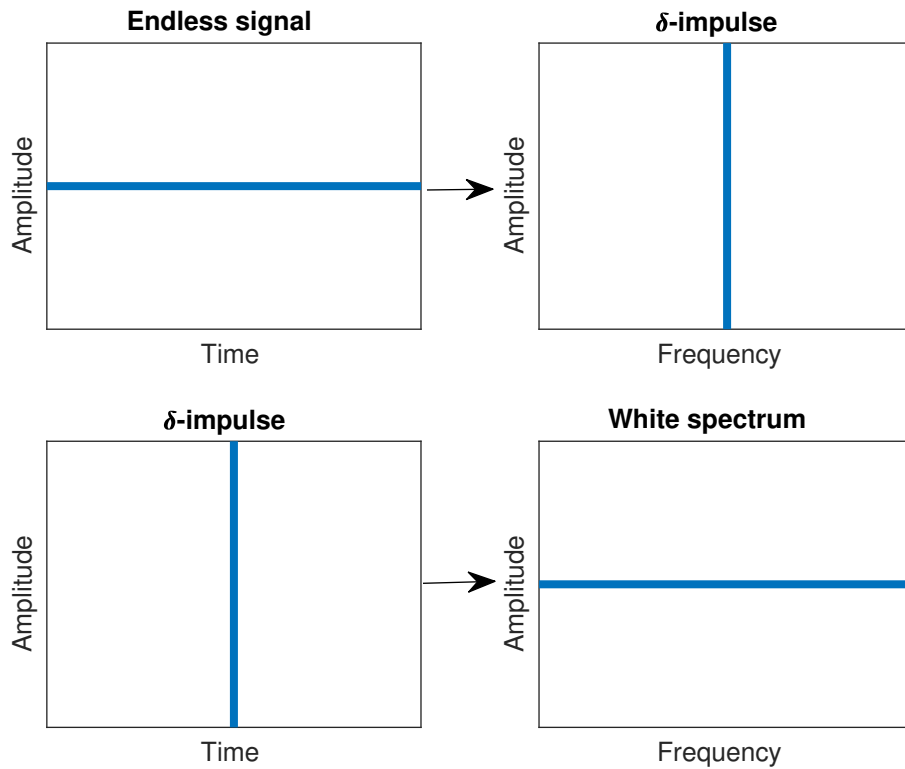


Figure 7: Heisenberg's uncertainty principle

Figure 8 by stacking two identical Ricker wavelets that have a small time shift.

When the time shift between the stacked signals is large the envelope of the spectrum does not change but there might still be notches in the spectrum. This is shown in Figure 9. However, the notches might disappear when stacking more than two signals, which is why they are not a reliable method to determine the correct stacking-velocity.

In the next chapters we will see whether this effect of Heisenberg's uncertainty principle can be used in applied seismic.

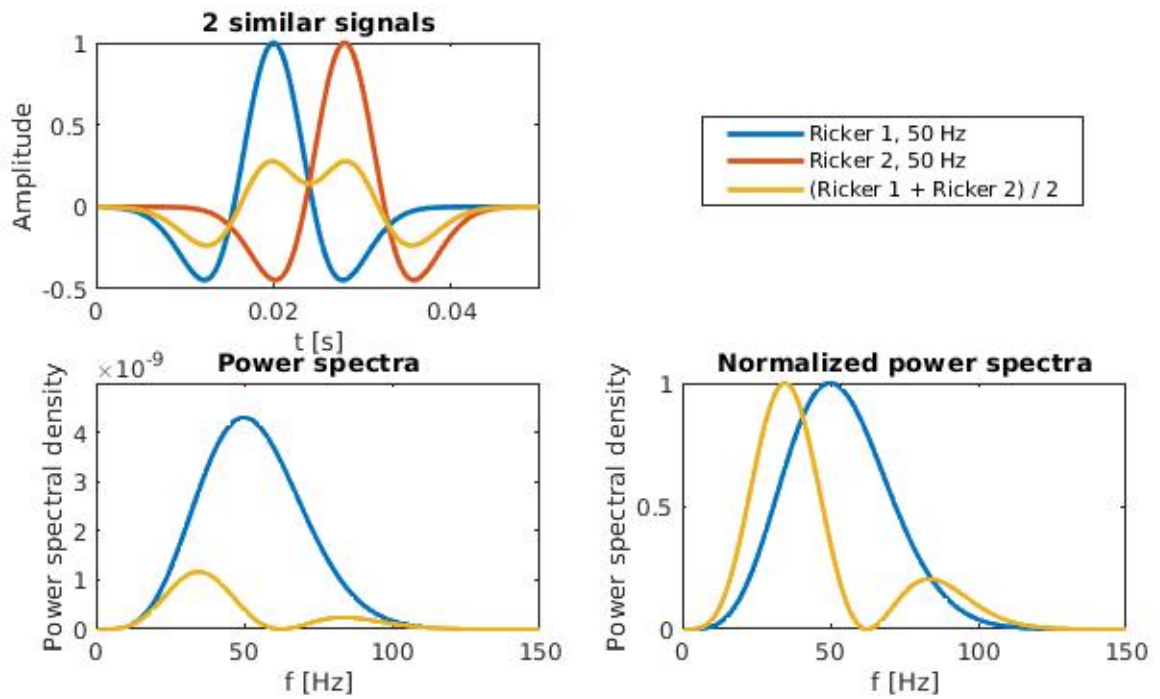


Figure 8: Stacking two identical signals that have a small time shift

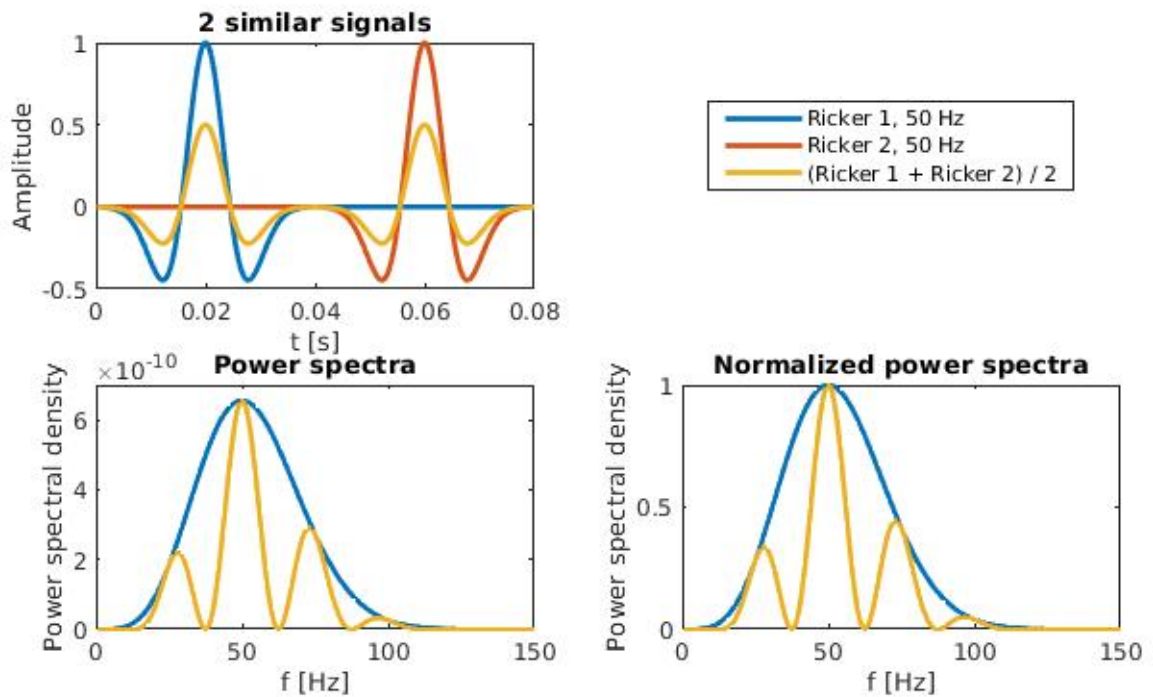


Figure 9: Stacking two identical signals that have a large time shift

parameter	value
offset interval	25 m
minimal offset	0 m
maximum offset	7325 m
recording length	5 s
sample frequency	500 Hz
main frequency	50 Hz
wave form	Ricker
reflector depth	1300 m
p-wave-velocity	1500 m/s

Table 1: Parameters of synthetic data

## 4 Data sets and processing

In this chapter I will explain the data sets that I used and the steps of data processing that I applied on the data.

I used the CMP 4300 from a TGS-data set, which was recorded in the Mediterranean sea. TGS is a company that provides the global energy industry with subsurface data. The version of the data set that I used had a time shift of 0.1256 s and a phase shift of 180°. I only corrected the time shift because the algebraic sign of the data has no influence on the semblance and bandwidth analysis .

Additionally, I created two synthetic CMP-gathers containing a single reflection of a Ricker-wavelet at a horizontal reflector which take the geometrical spreading into account. One data set is without noise and the other one contains Gaussian noise with a standard deviation of 10% of the maximum amplitude of the data set. To create the synthetic data I used the parameters in Table 1 which are chosen to approximate the field data. A difference between the synthetic data and the field data is the offset interval. For the synthetic data it is constant, but it varies between 12 m and 38 m in the field data. Due to the source gap the smallest offset in the TGS-data set is 163 m. The data sets are shown in Figure 10.

Except for the FFT function and some basic mathematical functions the used programs are written by myself in Matlab.

### 4.1 Amplitude adaptation, NMO-correction and stacking

First of all, I removed the geometrical spreading with Equation 6 and 7 and normalized each trace to its own maximum. Then I applied an NMO-correction for normal-moveout-velocities between 1300 m/s and 3500 m/s with an interval of 10 m/s. Afterwards, I muted in each trace all samples with an offset to target ratio  $x/z > 1$ . This was done twice, the first time with a constant velocity of 1500 m/s and the second time with a velocity profile, which was picked by TGS for CMP 4280. This velocity profile is shown in Figure 25 and was provided by Prof. Dr. Christian Hübscher. Computing the exact interval-velocities from the TGS-velocity profile would have been too complicated for me, therefore I estimated the depth with the following equation:

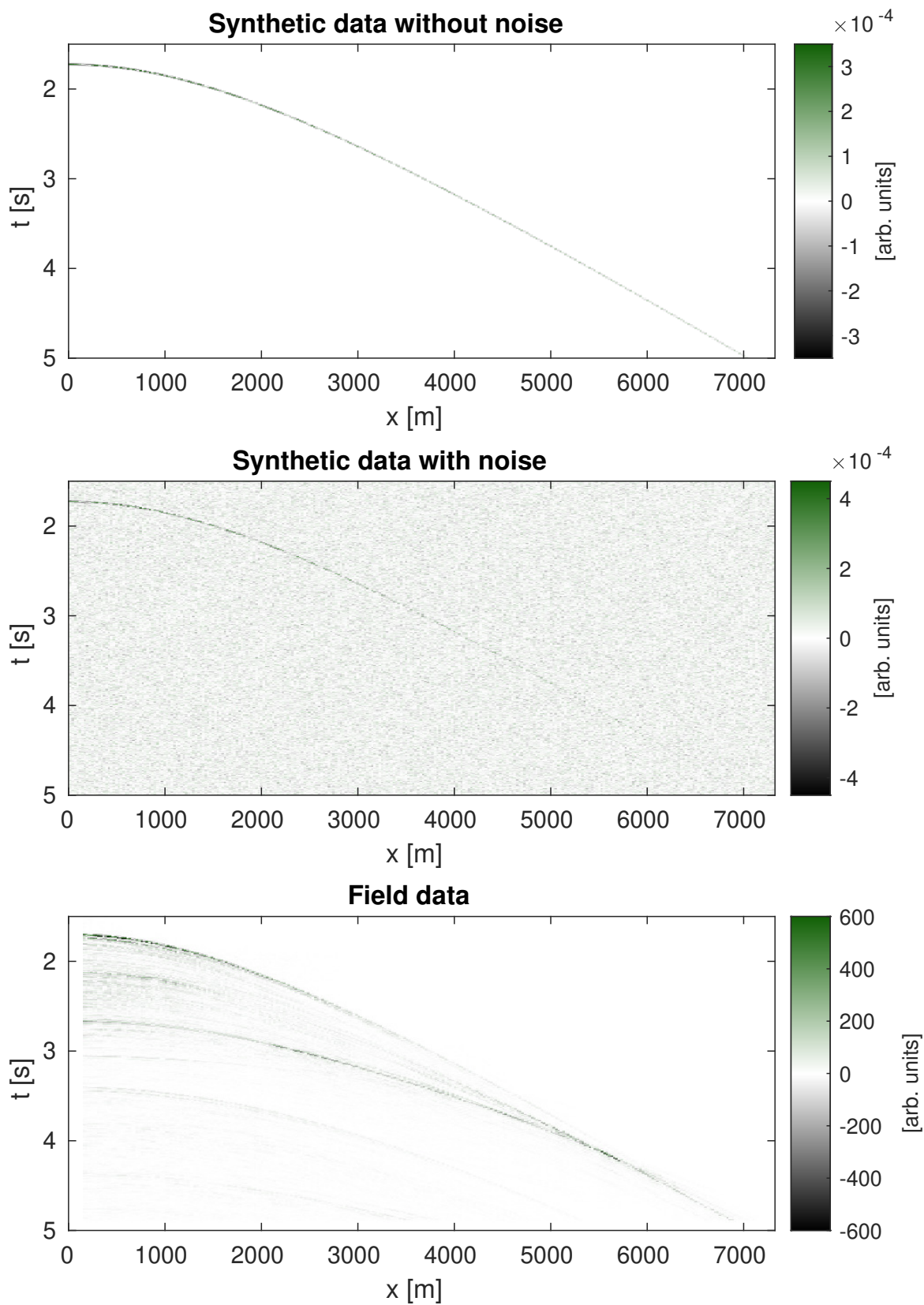


Figure 10: Datasets

$$z(t) \approx \frac{t}{2} \cdot v_{\text{NMO}}(t) \quad . \quad (18)$$

Notice that this depth conversion is only accurate enough to estimate which samples should be muted and should not be used for any other data processing.

The resulting differences in semblance and bandwidth are small and will be discussed in Section 5.2. Whenever the used velocity profile for the muting is not explicitly mentioned, the field data was muted with the velocity profile picked by TGS. For the  $v_{\text{NMO}}$  that straightens the first reflection best the unstacked NMO-corrected data sets are shown in Figure 11, 12 and 13.

To ensure that the muting of samples has no influence on the amplitudes of the stacked data, I divided every sample in the stacked data by the number of unmuted samples applied in the summation when stacking the data.

## 4.2 Semblance and power spectra

Our aim is to find the  $v_{\text{NMO}}$  that fits best to our data for different times. Therefore we have to divide the data set into small time windows in which we compute the semblance or bandwidth. If the chosen time window is too big the result is a bad resolution in time. If it is too small we do not have a good resolution in velocity and moreover we would not be able to compute power spectra that have an acceptable frequency resolution and shape. Experimentation revealed that in this case a time window of 0.1 s [ $\hat{=}$  50 samples] delivers good results. To get a smoother power spectrum I zero-padded the input of the FFT-function. This means that I added zeros to the input-vector so that its size is increased. For this I used the build in mechanism of the `Matlab` function `fft`. Tests revealed that zero-padding the vector to a length of 501 is a good compromise between calculation time and frequency resolution.

Knowing the applied steps in data processing we can now have a look at the results.

# 5 Results and discussion

I divided this chapter into two parts. In the first part we have a look at a time window that contains the seafloor reflection to develop the used bandwidth parameter. This is done for the synthetic data and field data. Afterwards the developed method is applied to the complete data set. Since the synthetic data sets only contain one reflection I restricted myself to the field data. Then I compare my results with the velocities that were picked by the company TGS.

## 5.1 One time window that contains the seafloor reflection

In this section we only have a look at one time window that contains the first reflection. I chose the time window  $t = [1.66 \text{ s}, 1.76 \text{ s}]$  shown in Figure 13. The reflections in the synthetic data and in the field data do not occur exactly at the same time because the synthetic data was only roughly adapted to the field data.

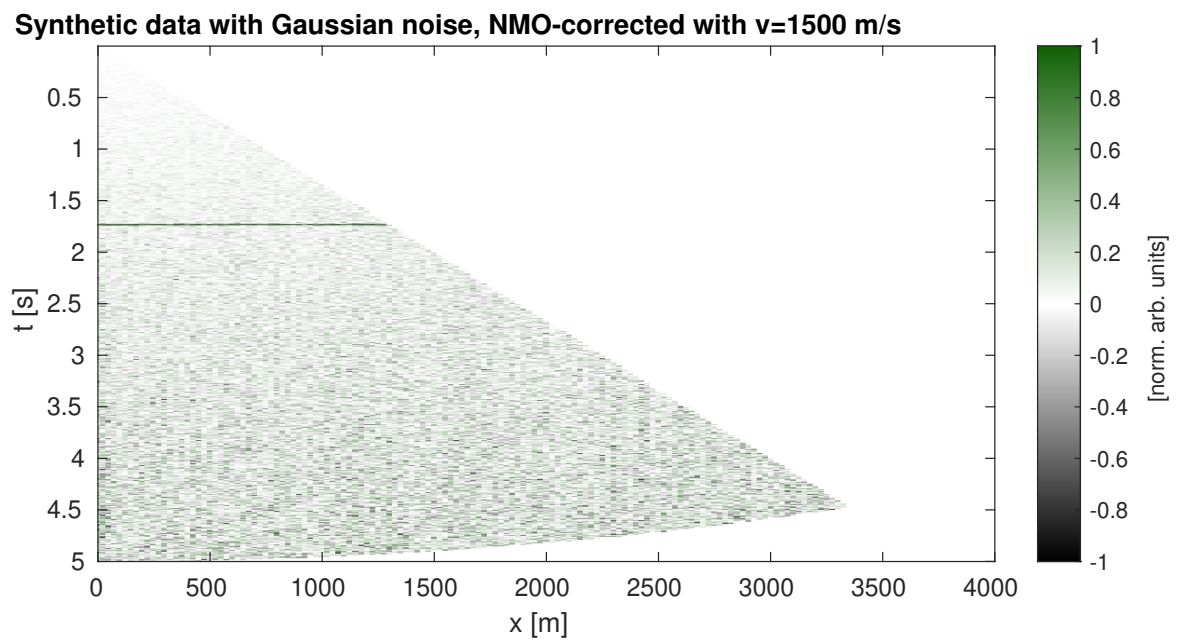
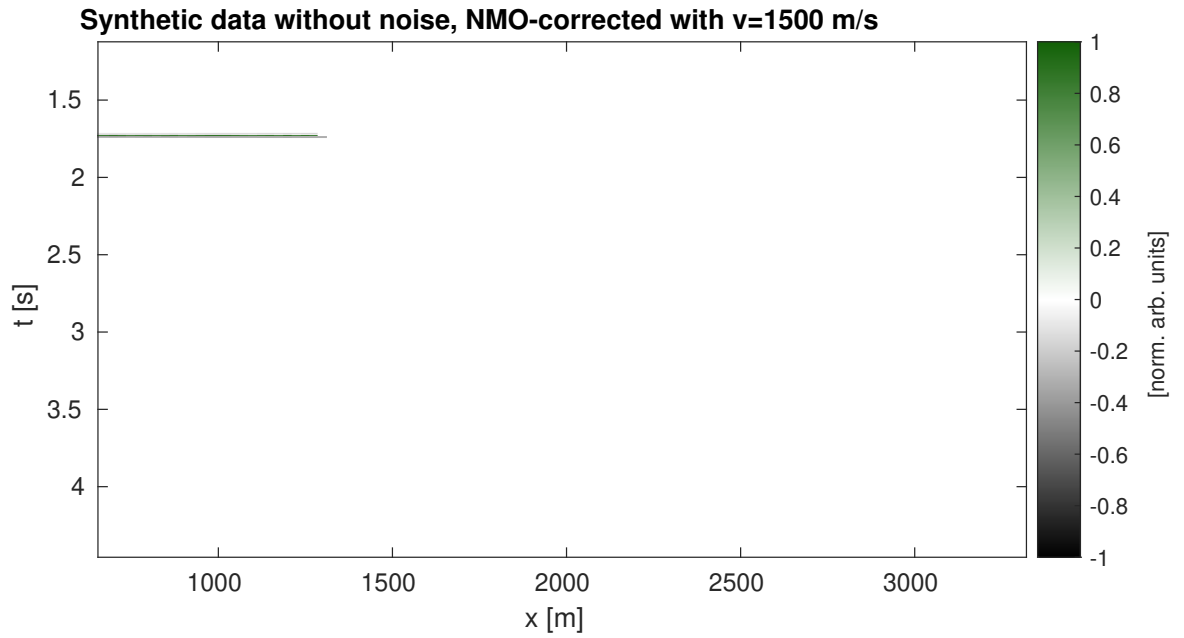


Figure 11: NMO-corrected unstacked synthetic data, close-up in Figure 13

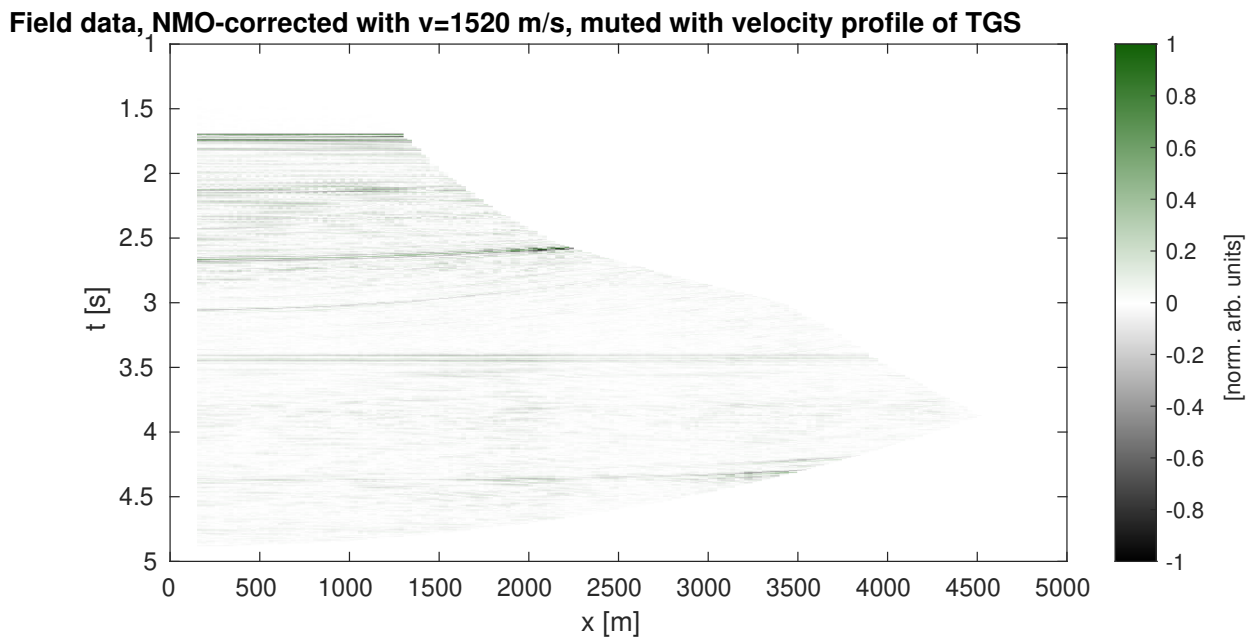
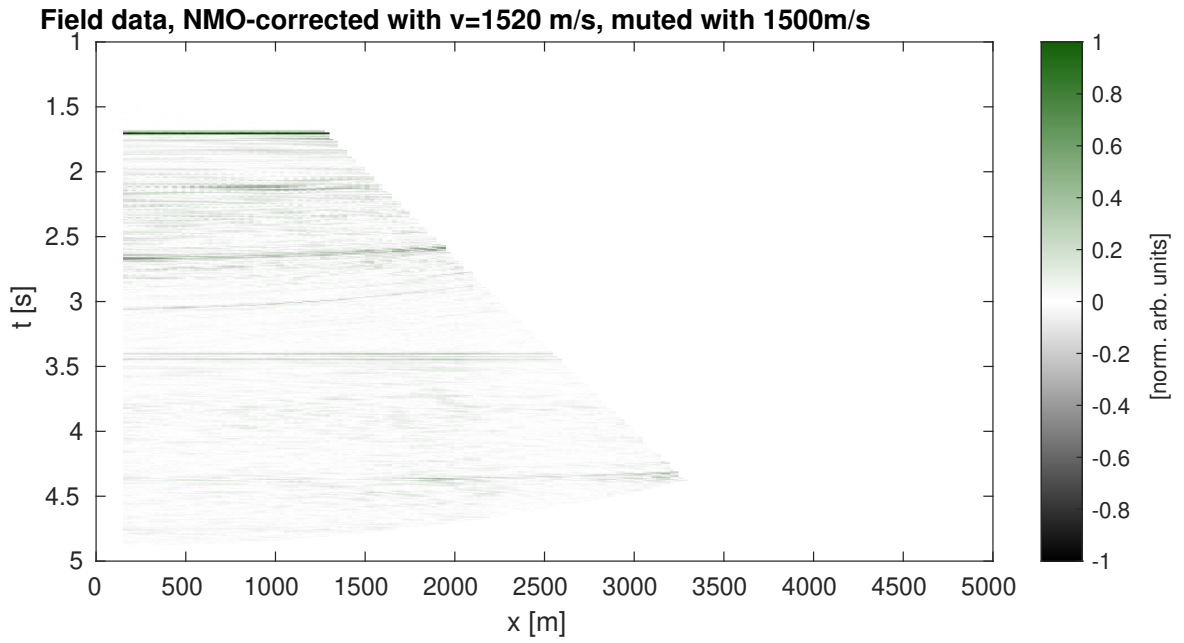


Figure 12: NMO-corrected unstacked field data, close-up in Figure 13

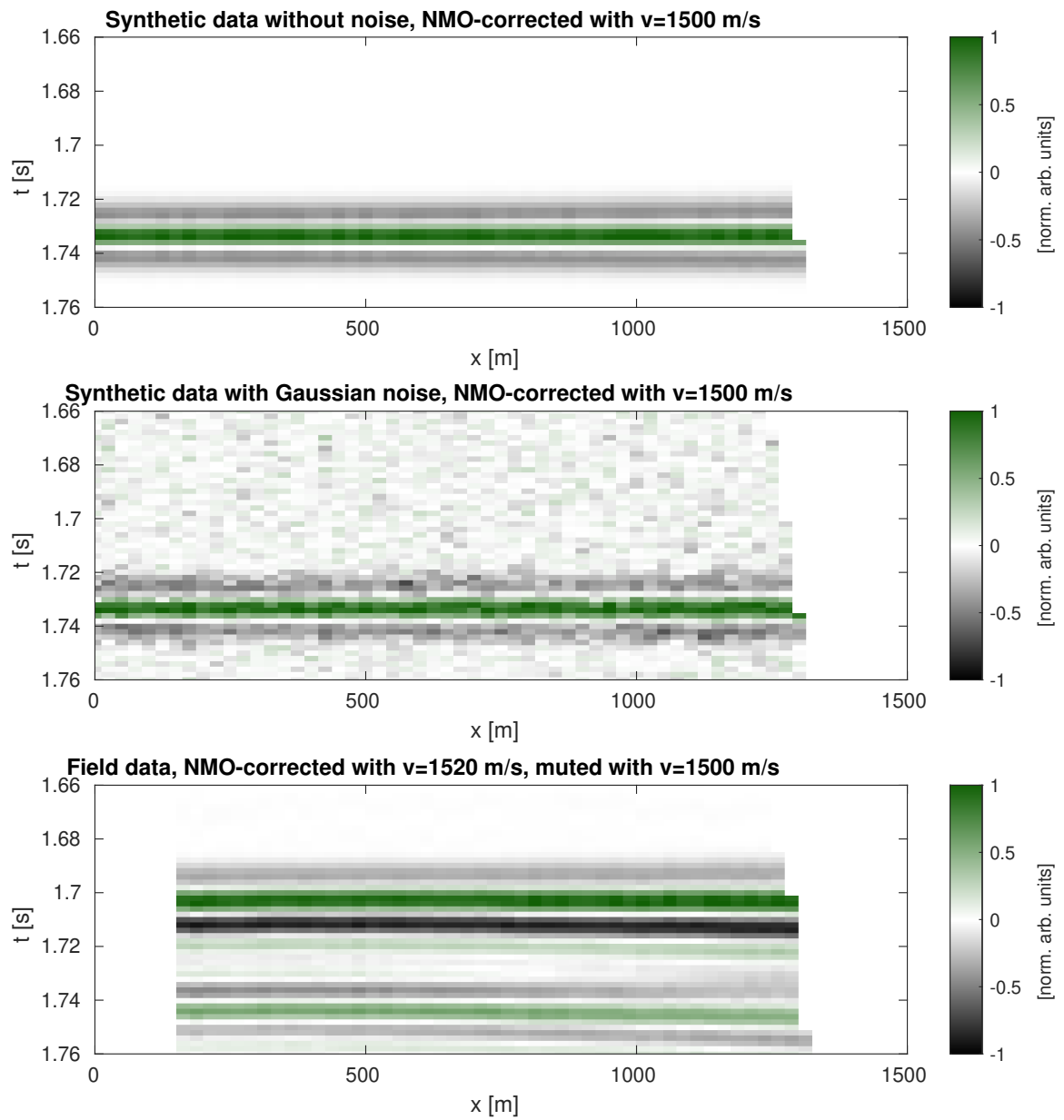


Figure 13: Close-up of the NMO-corrected unstacked data,  $t=[1.66 \text{ s } 1.76 \text{ s}]$

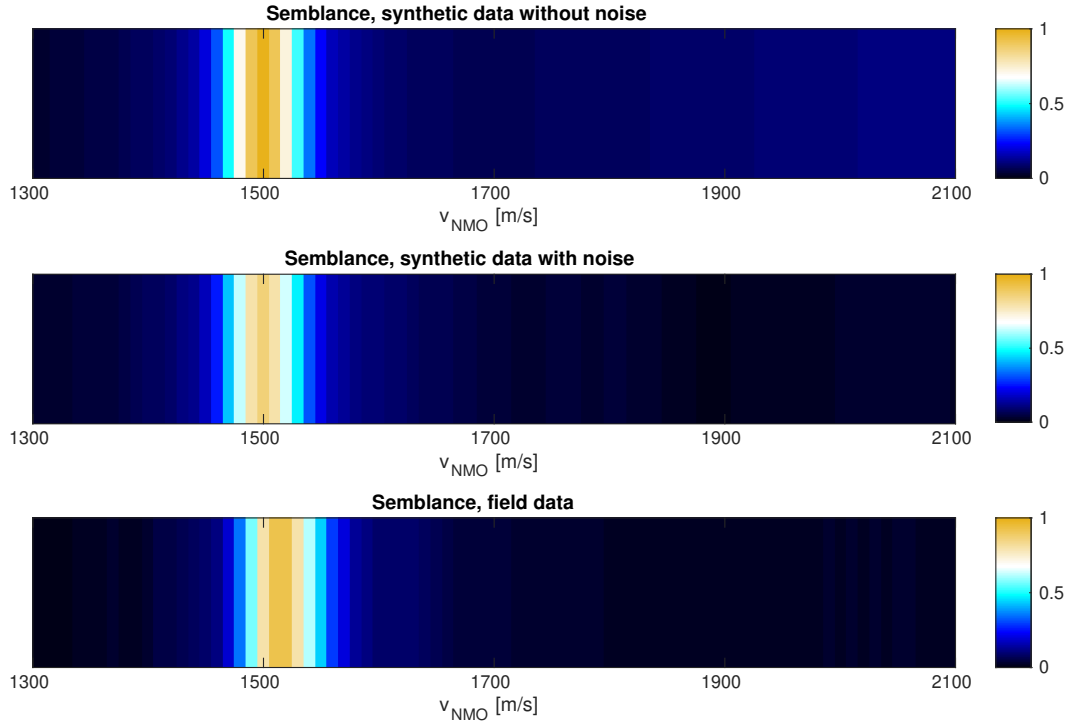


Figure 14: Semblance of the time window  $t=[1.66\text{ s } 1,76\text{ s}]$

### 5.1.1 Semblance

Figure 14 shows the semblance of the data in this time window. As expected, the best fitting velocity for the synthetic data is 1500 m/s. The maximum semblance for the noise-free data is slightly higher than in the noisy data. In the field data from the Mediterranean sea the best fitting velocity is 1520 m/s. This is a realistic value since it is in the range of seismic velocities in sea water. Small deviations can be explained by a slightly inclined reflector and density inhomogeneities in the water column.

### 5.1.2 Conventional definition of bandwidth

When looking at the power spectra of the stacked traces shown in Figure 15 we see a similar behavior to the semblance. The highest power spectral density for the synthetic data is at 1500 m/s and for the field data it is at 1520 m/s. But we also notice that if we only look at the maximal amplitudes of the spectra the best fitting velocity is not more focused than using the semblance method.

As a comparison Figure 16 shows the power spectra of the unstacked traces. They are very similar to the power spectrum of the stacked trace that is NMO-corrected with the best fitting velocity, but have higher power spectral densities. In the field data in time windows at larger times this difference is even larger, because it is not possible to straighten all reflections with one velocity.

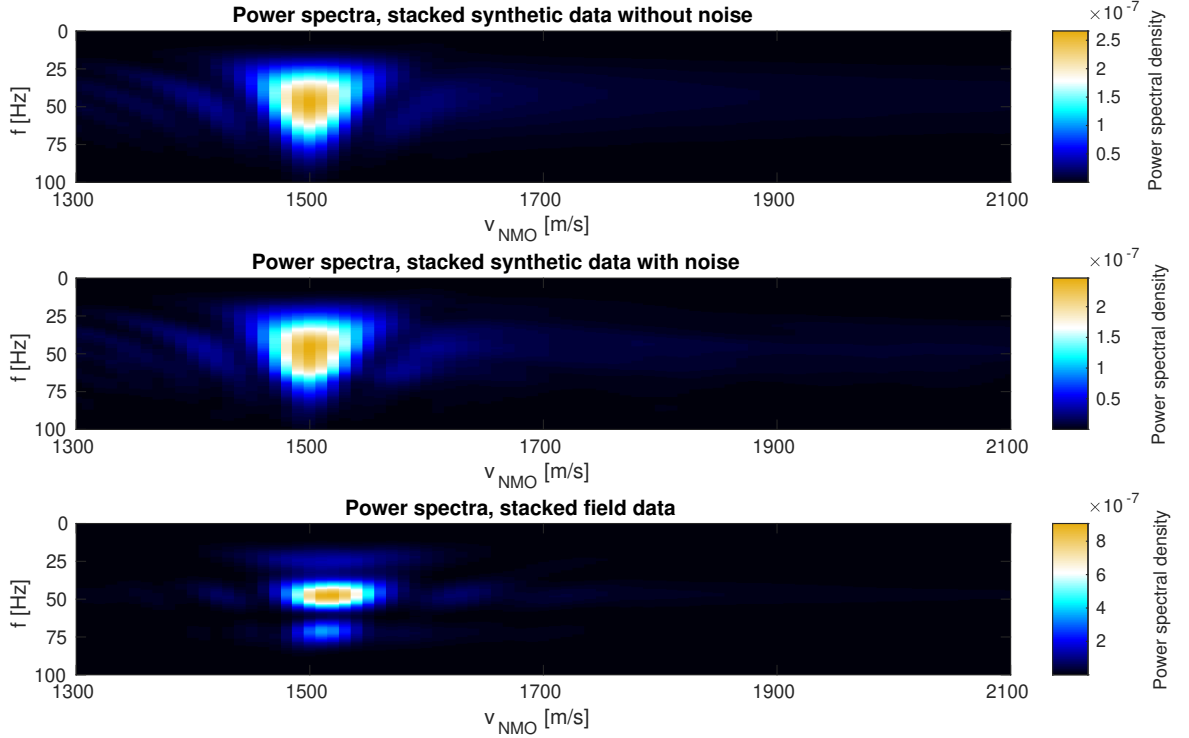


Figure 15: Power spectra of stacked traces,  $t=[1.66\text{ s } 1.76\text{ s}]$

The conventional definition of bandwidth is the frequency range around the maximum in which the power spectral density of the spectrum is above 50% of the spectrum's maximum [8]. First, we have a look at the normalized power spectra in Figure 17 to check whether this definition of bandwidth works out.

In the power spectra of the synthetic data we see that within a small range around 1500 m/s the bandwidth decreases for worse velocities. But when  $v_{\text{NMO}}$  deviates substantially from 1500 m/s the bandwidth does not differ from the bandwidth at 1500 m/s. The reason for this is that then the only significant difference between the stacked traces is the amplitude. This is shown in Figure 18.

In the field data it seems as if the bandwidth does not depend on the chosen velocity. The reason for this might be that there is more than one reflection and there is no velocity that perfectly straightens all reflections. Additionally, the power spectra of the unstacked traces already contain notches and they are not as smooth as the power spectra of the synthetic data.

The noise in seismic data is produced by many different sources which emit signals at different frequencies. Therefore the noise power spectrum is in a first approximation a white spectrum, which has an unlimited bandwidth. When stacking the traces with wrong velocities the amplitudes of the reflections become smaller, which increases the influence of the noise in the data. At large times the signal-to-noise-ratio is already small, which is why there the bandwidth might even increase when stacking the traces with wrong

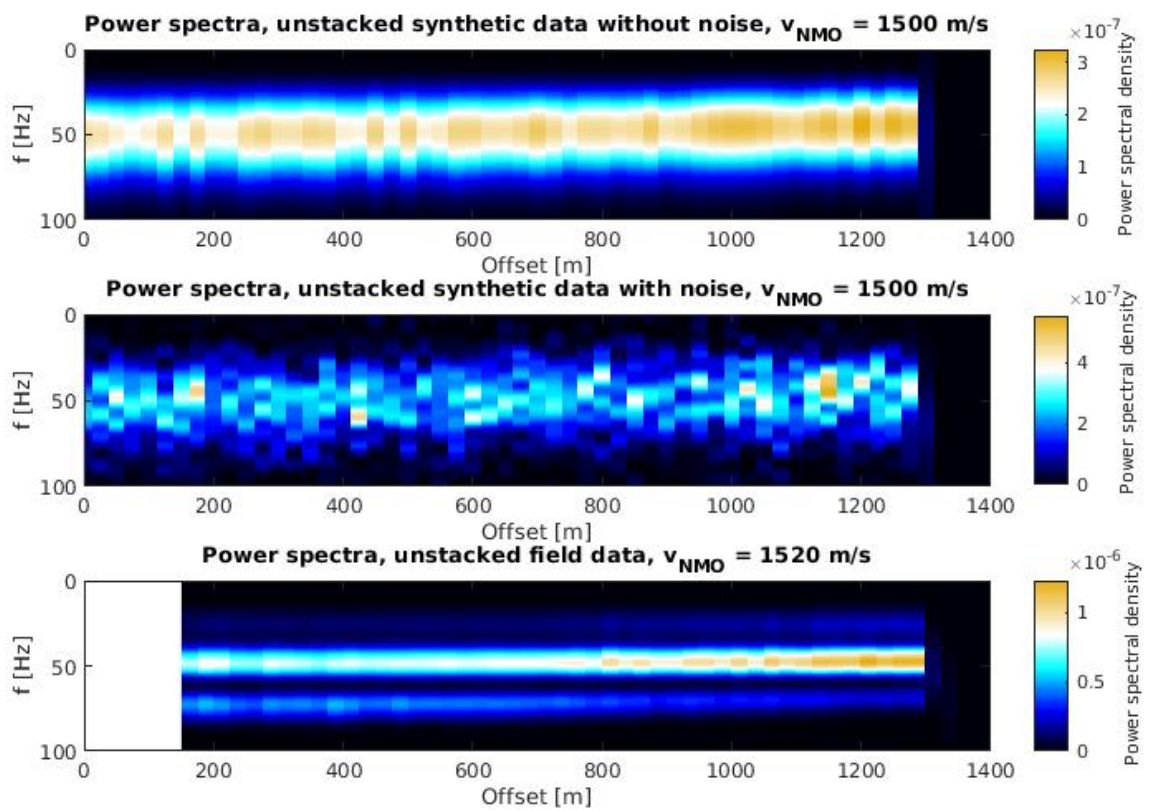


Figure 16: Power spectra of unstacked traces,  $t=[1.66$  s  $1.76$  s]

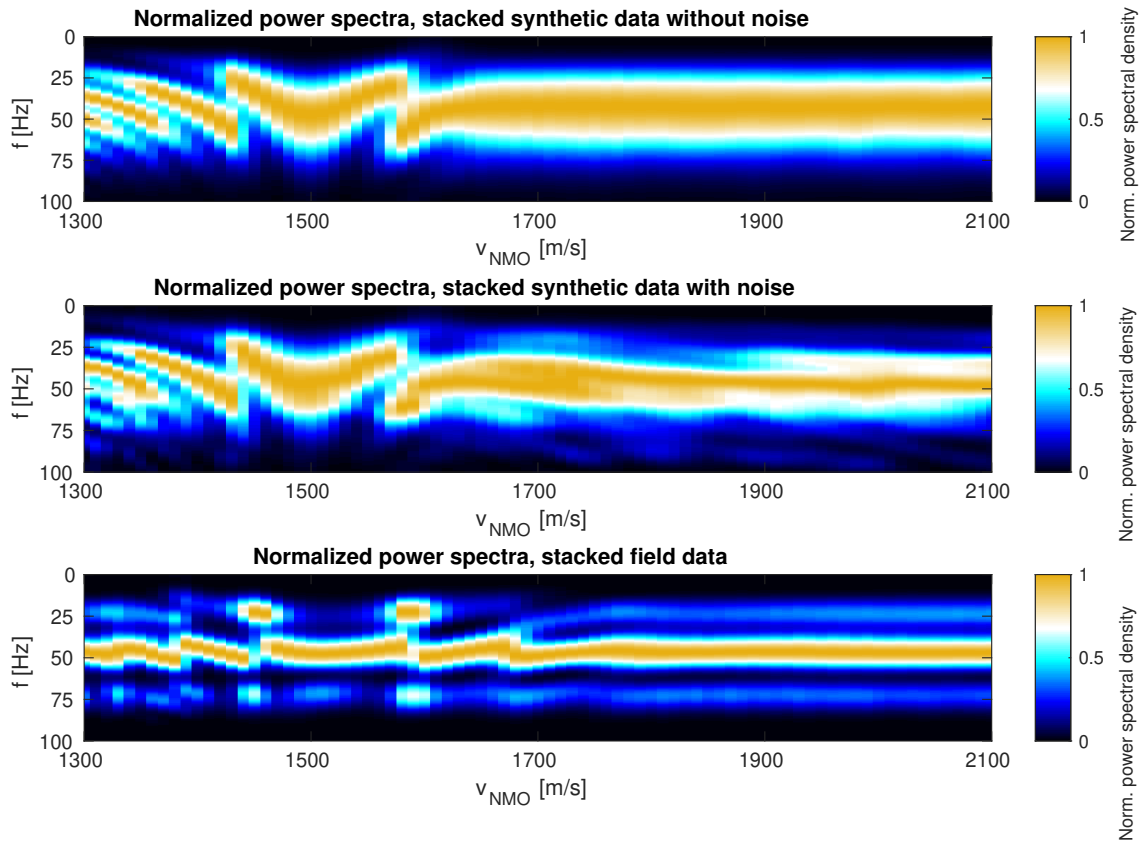


Figure 17: Power spectra of stacked traces normalized to individual maximum,  $t=[1.66$  s  
 $1.76$  s]

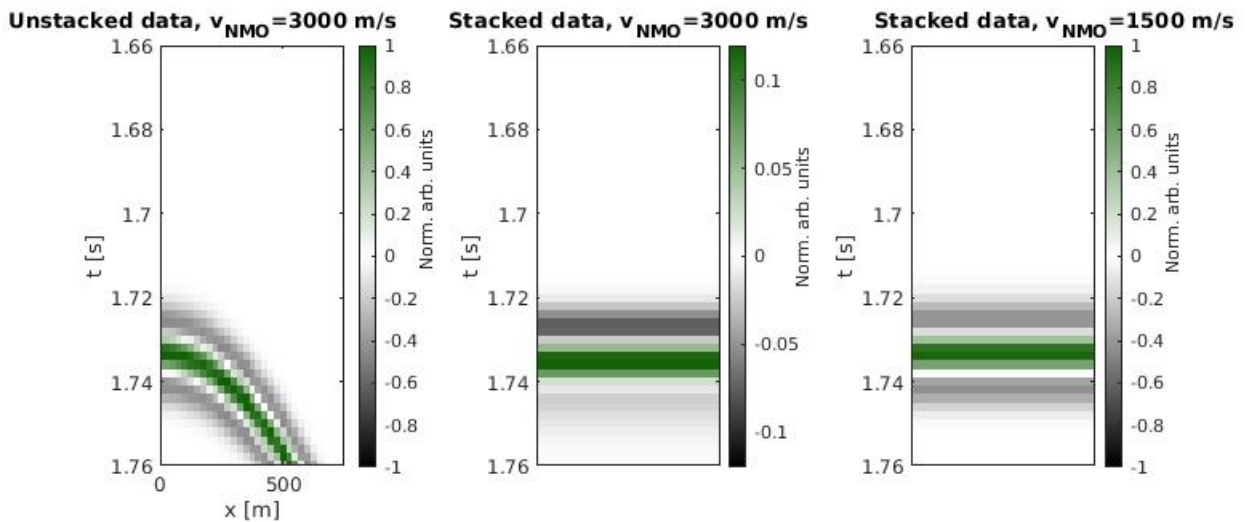


Figure 18: Left: Unstacked synthetic data, NMO-corrected with a very wrong velocity  
Center: Stacked synthetic data, NMO-corrected with a very wrong velocity  
Right: Stacked synthetic data, NMO-corrected with the correct velocity

velocities.

An idea to suppress the high bandwidth values at very wrong velocities would be to take only the traces with high semblance values into account, but as you can see by comparing Figure 14 and 17 this would result in a worse velocity resolution than only using the semblance.

### 5.1.3 New definition of bandwidth

Without considering the amplitudes we will not be able to use the bandwidth as an indicator for good or bad stacking-velocities. This is why I now define a bandwidth relative to a reference spectrum. This is shown in Figure 19.

Using this definition, bandwidth is the frequency range around the maximum in which the power spectral density of the spectrum is above 50% of a reference spectrum's maximum. By the selection of the reference spectrum there are different alternatives.

The first possibility is to use the average power spectrum of the unstacked traces (shown in Figure 16) as a reference spectrum. This would be an approach similar to the semblance. The problem is that the maximum semblance and therefore the energy-difference between the stacked and unstacked traces strongly varies with the time (see Figure 21): At small times the maximum semblance is around 1 and at large times the maximum semblance is smaller than 0.2. It would not be possible to use 50% of the reference spectrum's maximum for the definition of bandwidth, because then all bandwidths at huge times would be zero. When reducing the 50% to a smaller value, for example 10% or 5%, the influence of notches, noise and minor maxima would be too strong to get reliable results. Moreover this approach would require to compute a massive amount of power spectra, which results in much more computational effort. This is why I define the reference spectrum in a different way:

For each time window I use the spectrum that contains the highest power spectral density as a reference spectrum. This ensures that spectra of very wrong  $v_{NMO}$  have a bandwidth of 0 since their maximal power spectral densities are smaller than 50% of the maximum power spectral density in this time window. From now on bandwidth always refers to this bandwidth definition.

In Figure 20 the spectra's bandwidths of the stacked traces are computed for the time window  $t=[1.66\text{ s } 1.76\text{ s}]$ , which contains the sea floor reflection. Because of the already in the unstacked data existing notches the field data's bandwidth is smaller than the synthetic data's bandwidth (see Figure 15). We see that the bandwidth method delivers similar results compared to the semblance method (see Figure 14). The correct velocity is not more focused. But maybe the bandwidth provides better results than the semblance at greater times when not all signals can be straightened with the same  $v_{NMO}$ .

## 5.2 Entire trace length

Now we do not only look at one 0.1 s window but at the entire recorded time. Since in the synthetic data there is only one reflection I restricted myself to the field data in this

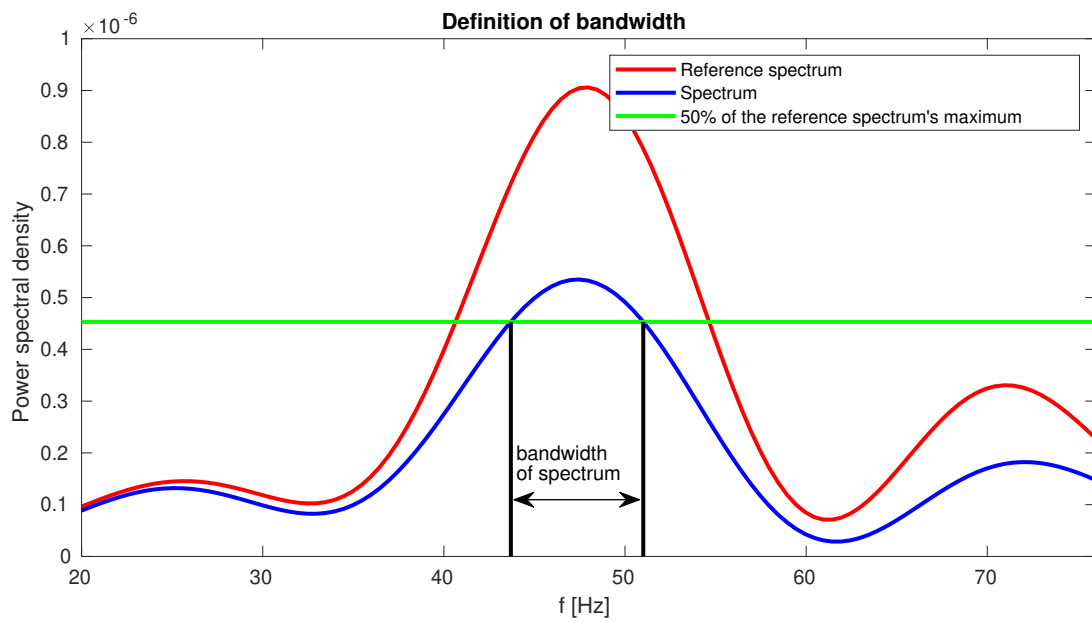


Figure 19: Applied definition of bandwidth

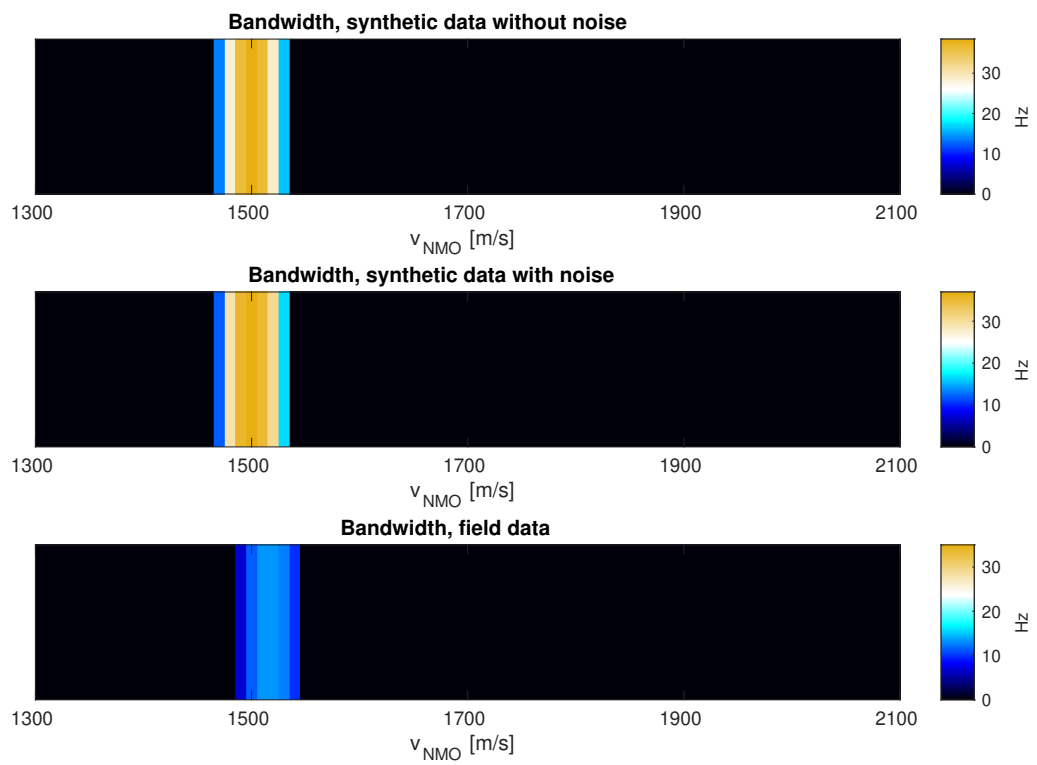


Figure 20: Bandwidth of the time window  $t=[1.66 \text{ s } 1.76 \text{ s}]$

section. I computed the semblance and bandwidth every 0.25 s and used for this 0.1 s windows centered around the declared time. Because of the extend of the time window the time resolution is limited. Therefore it would not make sense to choose time intervals that are much smaller than 0.1 s for computing the bandwidth and semblance. Tests revealed that an interval of 0.25 s delivers good results. The semblance and bandwidths are illustrated in Figure 21.

The first thing that catches your eye is the bad velocity resolution in semblance and bandwidth between 0 s and 1.3 s. There the data set contains only noise with low amplitudes, which in general interferes destructively when being stacked. Therefore the semblance values are small. We compute the bandwidth relative to the  $v_{\text{NMO}}$  that fits best, so in every time window we always get bandwidths  $> 0$  for some velocities. The high bandwidth and velocity values at very small times are boundary effects due to muting. The velocity values before 1.3 s can simply be ignored, since the seismic velocity in water is roughly known.

At times between 1.3 s and 1.6 s the semblance- and the bandwidth method deliver clear normal-moveout-velocities, even though the sea floor reflection occurs at later times. These  $v_{\text{NMO}}$  are between 1500 m/s and 1540 m/s and therefore plausible. This can only be explained by strong density variations in the water column that cause reflections with small amplitudes.

The seafloor-reflection occurs at 1.7 s. Time windows that are slightly before 1.7 s only contain the seafloor-reflection if a too small  $v_{\text{NMO}}$  is chosen. Then the seafloor reflection is over-corrected. The seafloor reflection has much higher amplitudes than the noise and the reflections of the water column. Therefore the highest bandwidth values are reached when the time window contains the seafloor reflection. In general this is not a problem, since the water depth is known generally.

Until 2.7 s it is easy to identify the velocity that straightens the reflections best, regardless of whether you look at the semblance or at the bandwidth. After 2.7 s it is not clear where to pick the velocities when using the semblance whereas the bandwidth localizes  $v_{\text{NMO}}$  more clearly. For better comparability of semblance and bandwidth Figure 22 shows a close-up. There you can see that the bandwidth also shows at which times strong reflections occur, whereas the semblance has a line of high values that is not clearly delimited in time. The three orange bandwidth values mark the huge impedance contrasts at the seafloor, the salt top and the salt bottom [7] (see Section 6.1).

From 3.3 s on there are multiples. They are additionally reflected at the water surface and afterwards at the seafloor. For them semblance and bandwidth deliver similar results.

We defined the bandwidth relative to the velocity that produces the highest power spectral density value. From 3.3 s on, this is the velocity that straightens the multiple reflections. Because of their high amplitudes we are not able to identify the single reflections which have smaller amplitudes. For this we would have to take the spectra of velocities assumed not to belong to the multiple as reference spectra. This is done in Figure 23. The bandwidths within the white box are computed relative to reference spectra that belong to velocities within the range of [2000 m/s, 3500 m/s]. Now the bandwidth clearly defines the velocity range in which we have to pick  $v_{\text{NMO}}$  whereas the semblance does not deliver

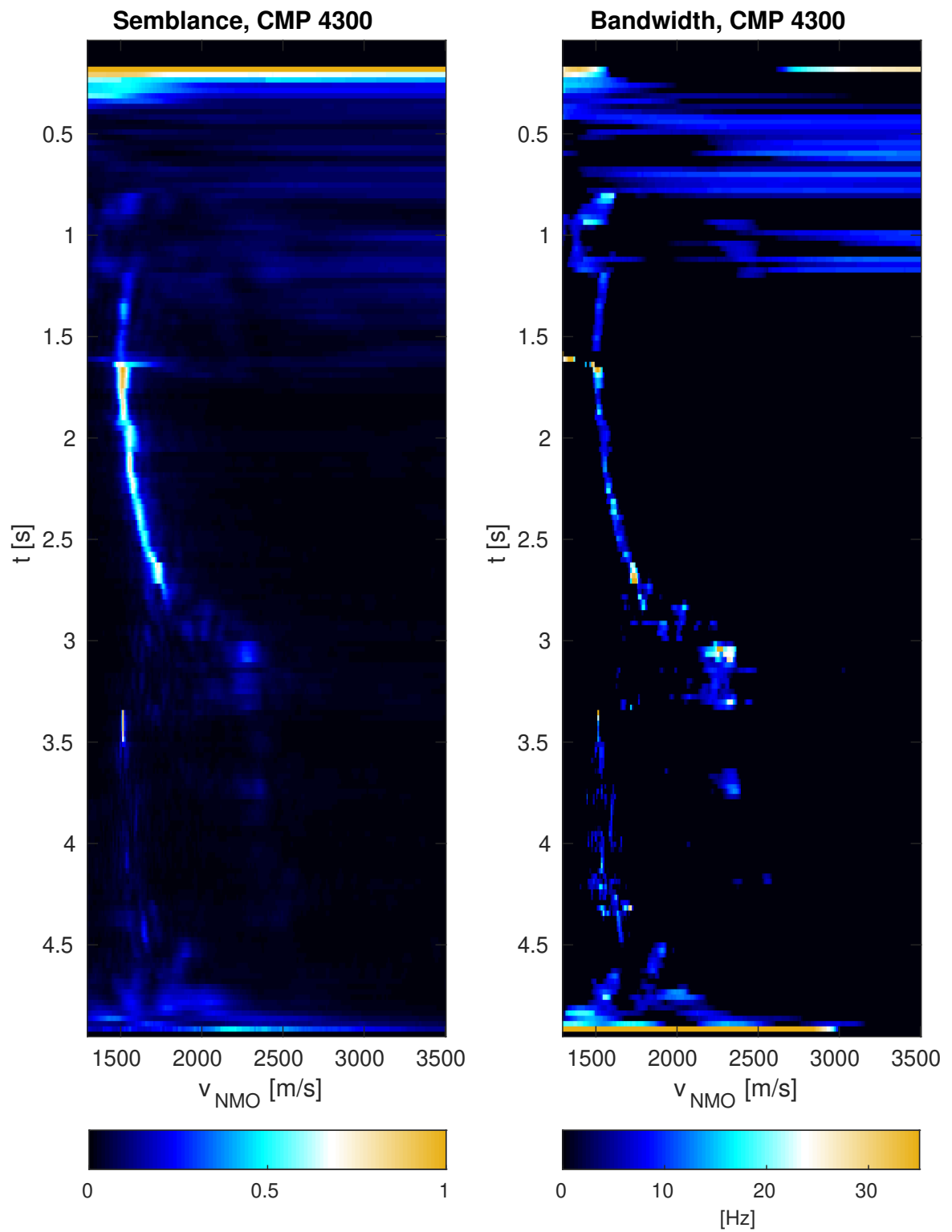


Figure 21: Semblance and bandwidth of field data

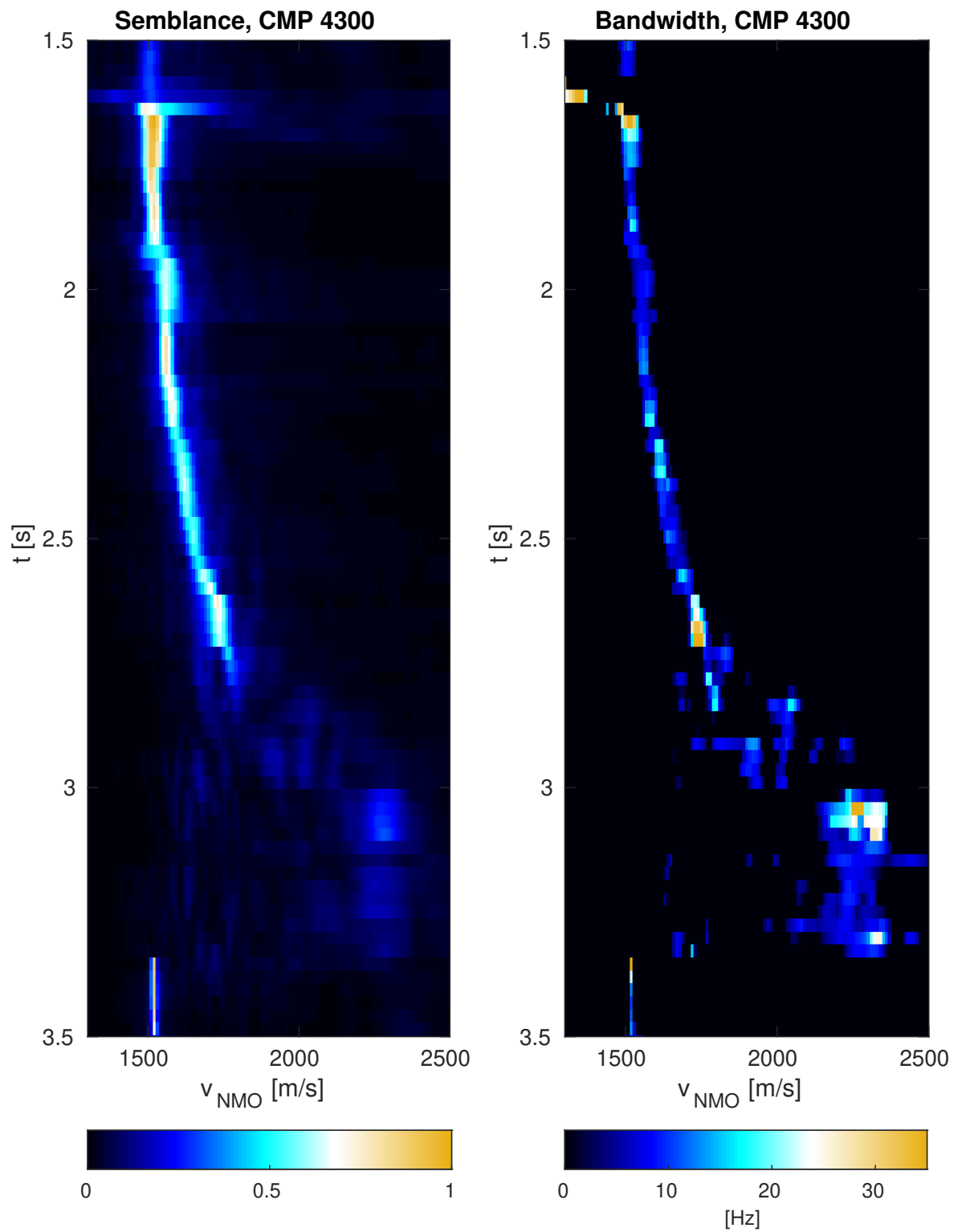


Figure 22: Semblance and bandwidth of field data, close-up

distinct velocity values.

At times greater than 4.5s there is no recorded data in traces with large offsets because the NMO-correction shifts the traces to smaller times (Figure 11). Therefore the moveout is way too small to make a good velocity analysis. The bandwidth and semblance values are not significant at these times.

Now we can have a look on how much the number of muted samples affects the results. Figure 24 compares the semblance and bandwidth values when different amounts of samples are muted. The two velocity profiles that were used for muting are the ones that were introduced in Section 5.1. The semblance has slightly higher values when using 1500 m/s for muting. Both, semblance and bandwidth, have a worse velocity resolution when using 1500 m/s for muting. The missing moveout affects the bandwidth stronger than the semblance.

## 6 Quality control

### 6.1 Picked velocities

Now we will check whether the computed bandwidth values make sense by roughly picking velocities by hand and comparing them to velocities that were picked by TGS at CMP 4280. The CMP-interval is 12.5 m [9] which means that CMP 4280 and CMP 4300 have a distance of 250 m in between.

Figure 25 shows the normal-moveout-velocities that were picked by TGS at a CMP nearby and my picked  $v_{\text{NMO}}$  for the used CMP. To get a rough idea of the actual seismic velocities that belong to the normal-moveout-velocities I computed them with the dix-inversion. Figure 26 shows that the inclination of the layer boundaries are small and therefore the conditions for the dix-inversion are fulfilled.

The high interval-velocities between 2.7s and 3s can be explained by a layer of salt [7]. The huge impedance contrasts at the top and bottom of the salt cause strong reflections, which result in high bandwidth and semblance values. In the time interval [2.6s 3s] my picked normal-moveout-velocities and the ones of TGS differ significantly. There the TGS-velocities do not fit to computed the semblance and bandwidth.

To get a very rough idea of how large the depth differences at the top and the bottom of the salt between both velocity models are I use the following equations:

$$\Delta z \approx t_2 v_{\text{NMO}, 2} - t_1 v_{\text{NMO}, 1} \quad (19)$$

$$\Delta z_{\text{Top of salt}} \approx 2.7 \text{ s} \cdot 1740 \text{ m/s} - 2.54 \text{ s} \cdot 1700 \text{ m/s} \approx 380 \text{ m} \quad (20)$$

$$\Delta z_{\text{Bottom of salt}} \approx 3.04 \text{ s} \cdot 2270 \text{ m/s} - 2.99 \text{ s} \cdot 2270 \text{ m/s} \approx 110 \text{ m} \quad (21)$$

The assumption for this equation is that the reflectors are not strongly inclined but even then the resulting depth is not exact at all. These depth differences would mean an average boundary inclination of above 50° for the top of the salt and above 15° for the bottom of the salt. Such high inclinations are highly unlikely and break the condition for

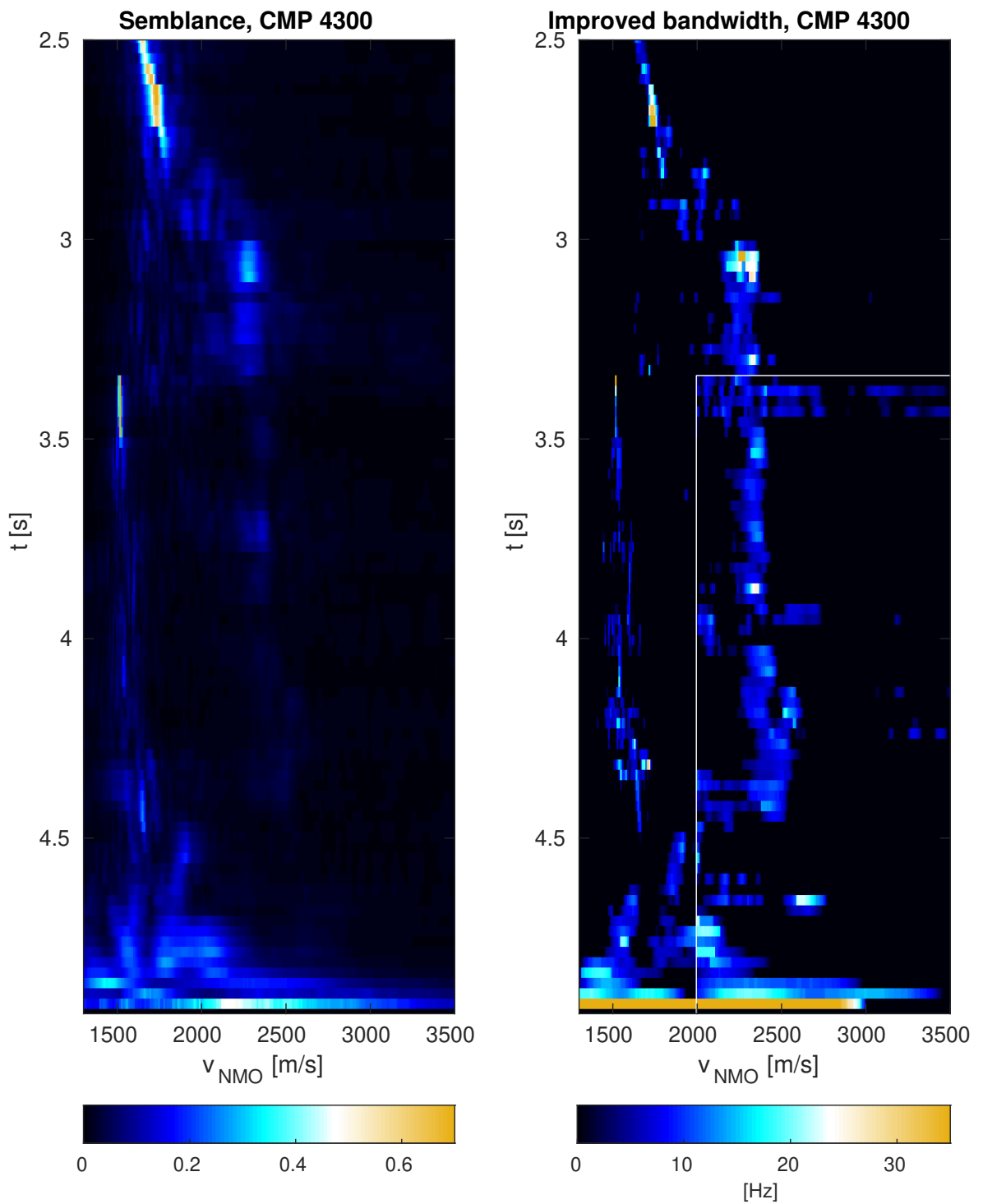


Figure 23: Semblance and bandwidth of field data, close-up  
 White box: Only spectra with velocities above 2000 m/s are used as reference spectra

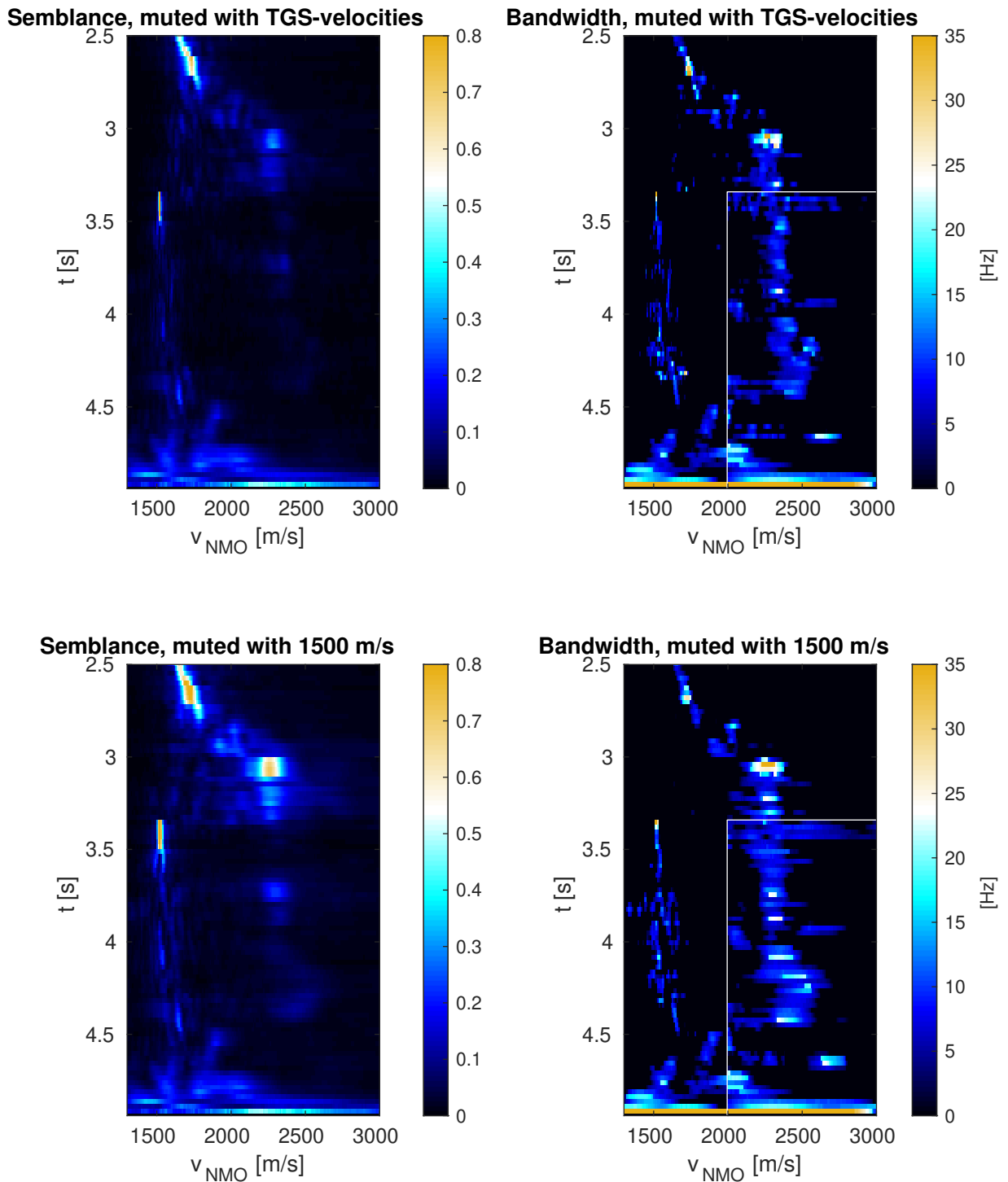


Figure 24: Semblance and bandwidth of field data, close-up  
 Top: The TGS-velocity profile was used to mute samples  
 Bottom: 1500 m/s was used to mute samples

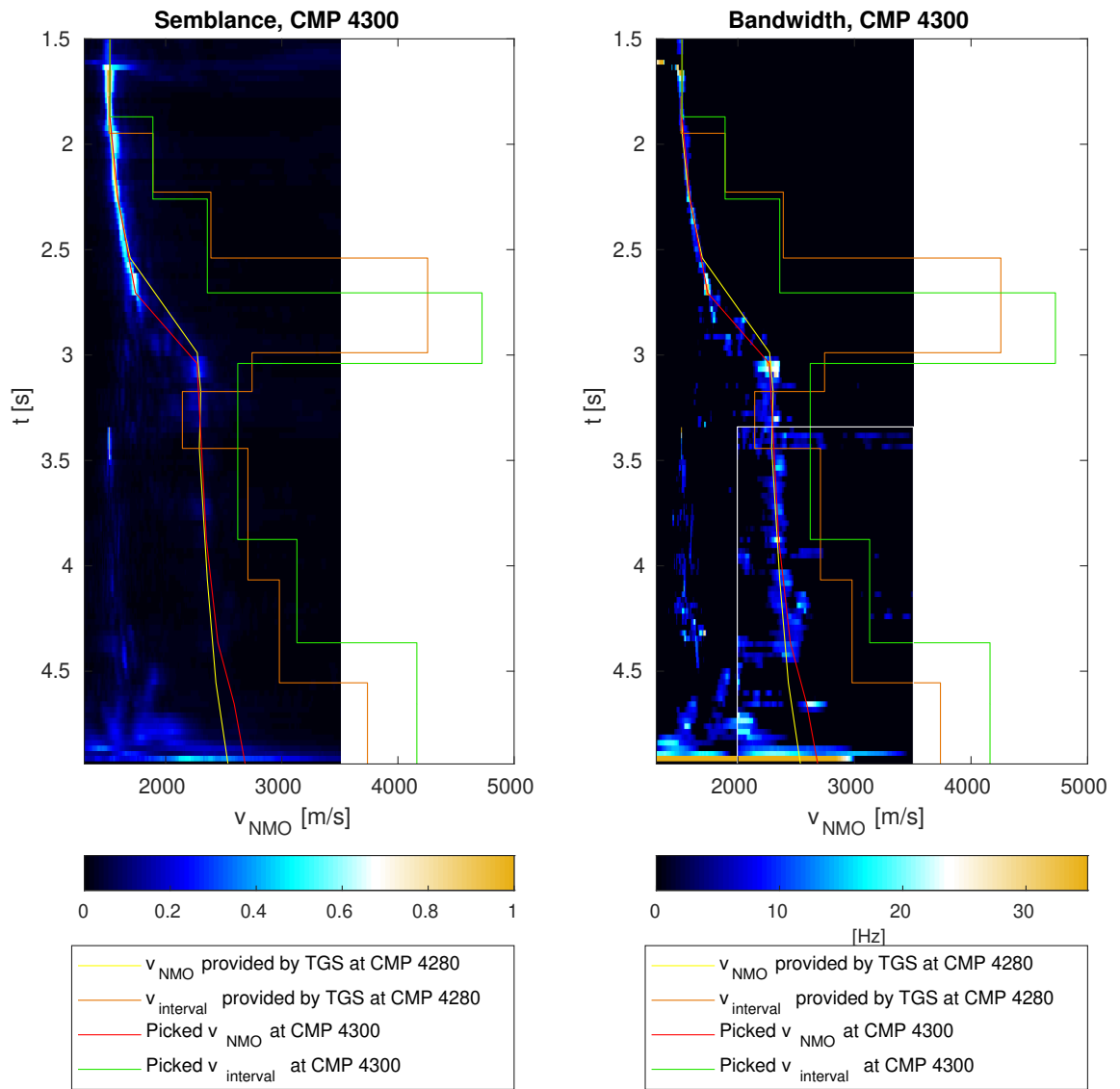


Figure 25: Semblance and bandwidth of field data with picked velocities, close-up

applying Equation 19. Therefore the depth differences are uncertain. The huge velocity deviations between the two profiles are further differences in Section 6.2 and 6.3.

At times larger than 4.5 s I also picked different velocities than TGS. Probably this is because only a part of the data set was given to me and the original data set is longer than 5 s. Therefore TGS had more moveout at large times, so their velocity resolution at these times is better.

## 6.2 Migrated data

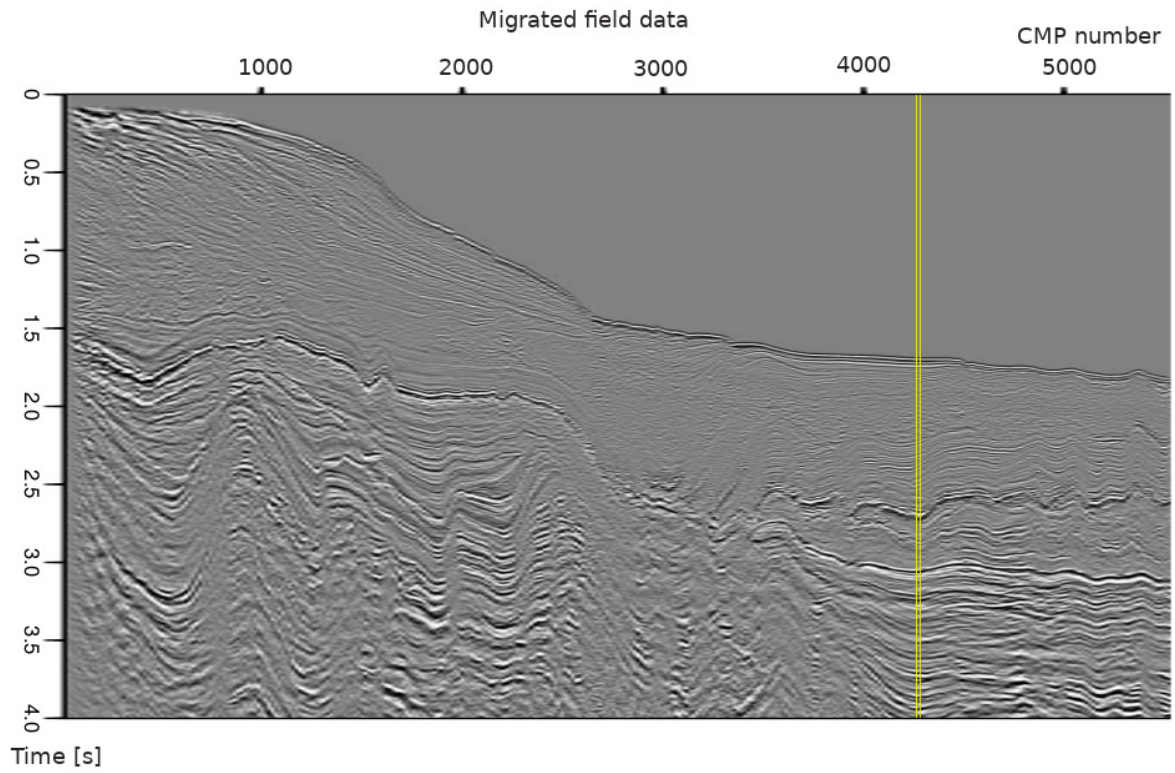
Figure 26 shows the migrated field data provided by TGS. The yellow lines roughly show the position of CMP 4280 and CMP 4300. At these CMPs the reflectors are approximately horizontal. It can therefore be assumed that the migration did not significantly change the times at which the reflections occur [8]. The two-way times of the reflections at the top and bottom of the salt in the migrated data fit to the velocity profile that I picked. The velocity profile of TGS shows significant differences. Probably there is a mistake in the file from which I got the picked velocities of CMP 4280. To confirm this I use the program `Seismic Unix` to check, whether the two velocity profiles straighten the reflections.

## 6.3 Seismic Unix

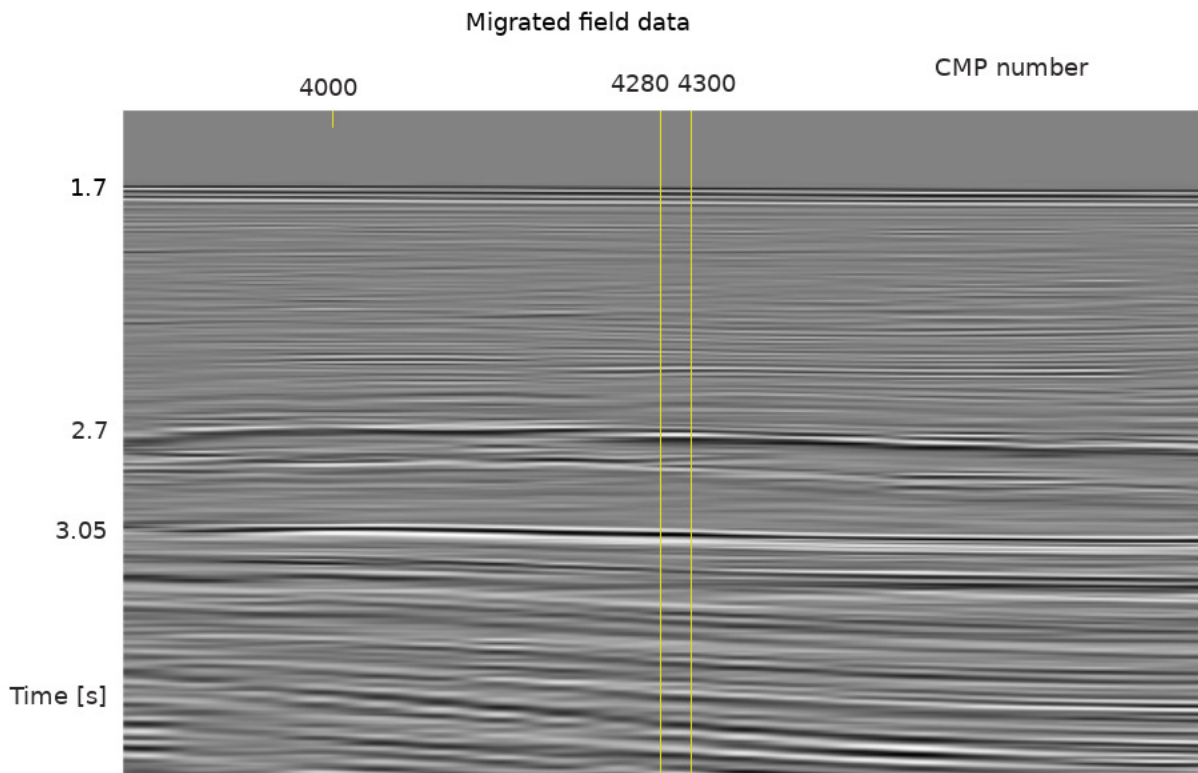
The CMP-gather is now NMO-corrected with the Program `Seismic Unix`. For this the picked velocities of Figure 25 are used. The figures are created with the function `suxwigb`. `Seismic Unix` mutes traces with huge offsets automatically which leads to a not very reasonable looking muting pattern. This does not affect whether the reflections are in phase or not and therefore it is not problematic. The red line roughly shows which samples I muted for the velocity analysis (see also Figure 12). Figure 27(a) and 27(b) show all CMP-traces. The biggest difference between these images occurs at around 2.7 s. At these times the differences between my picked velocities and the velocities that were picked by TGS at CMP 4280 reach the maximum. Figure 28(a) and 28(b) show a close-up around 2.7 s to determine which velocity profile straightens the reflections best.

Except for large offsets my picked velocities straighten nearly all reflections with high amplitudes well whereas the TGS-velocities in the time window [2.6 s, 3 s] are not suitable. Outside this interval the reflections are also straightened well when using the TGS-velocities. There the TGS-velocity profile and my picked velocity profile nearly match.

The conclusions are that at CMP 4300 the layer boundaries are approximately horizontal and probably there is a mistake in the file that contains the picked velocities of TGS. Using my picked velocity-profile, which fits to the computed semblance and bandwidth values, the reflections are straightened well. Therefore my programs that compute the semblance and bandwidth work properly.

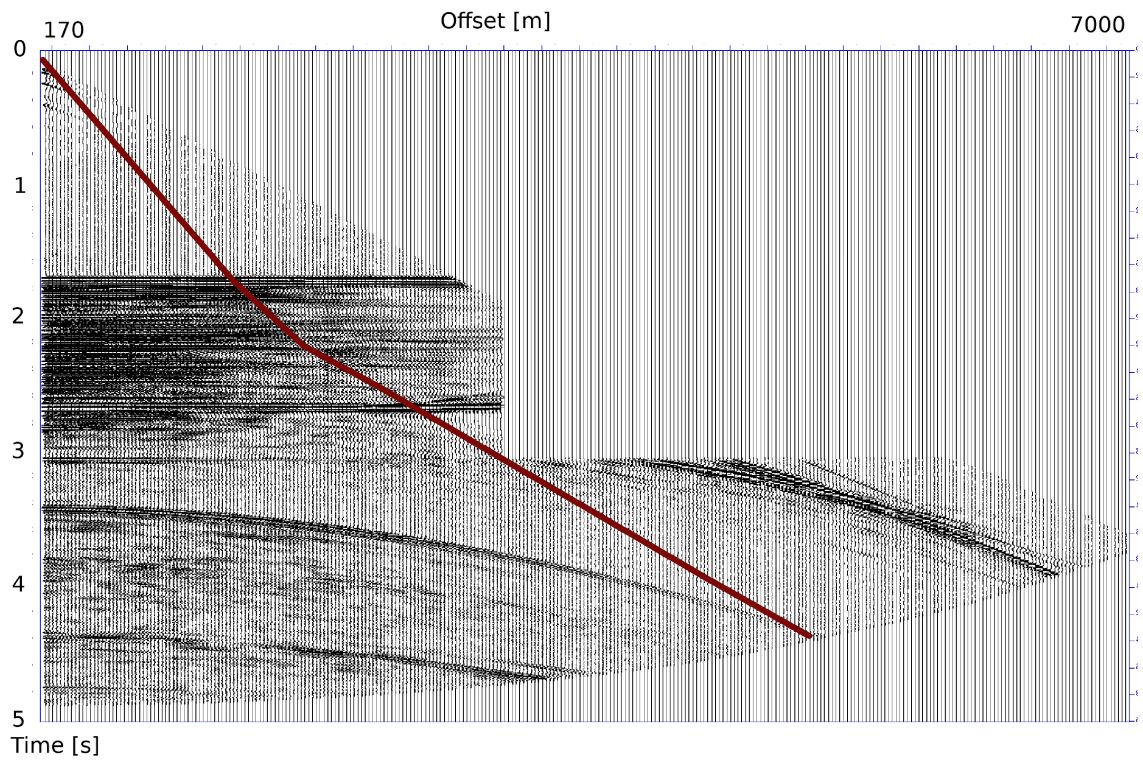


(a) Migrated field data, created by TGS

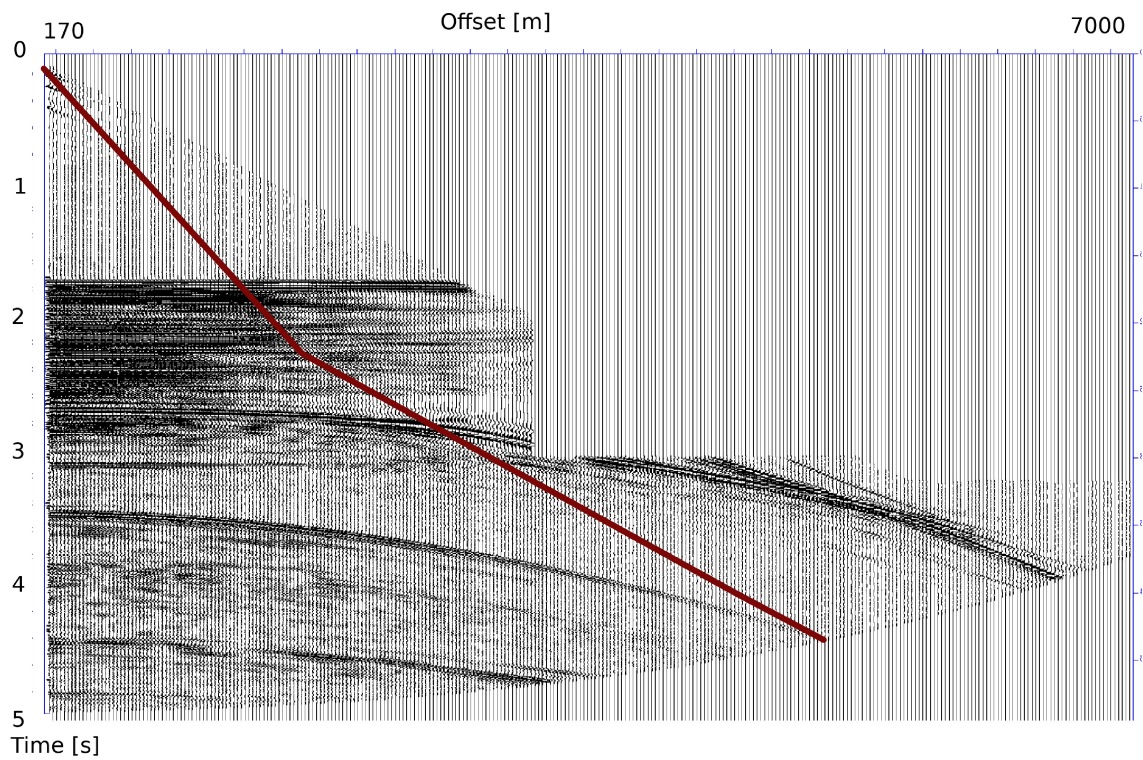


(b) Migrated field data, created by TGS, close-up

Figure 26: ]  
Migrated field data, provided by Prof. Dr. Christian Hübscher, changed by Ben Schmidt

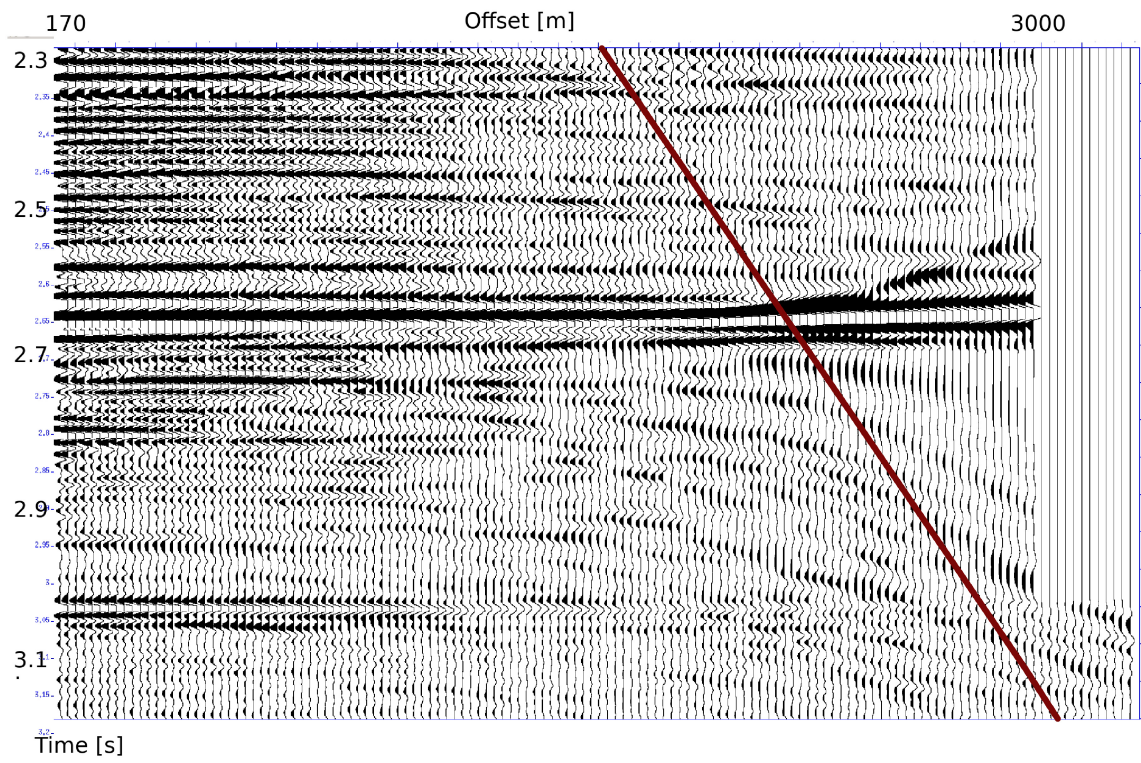


(a) NMO-corrected with velocities that were picked at CMP 4300

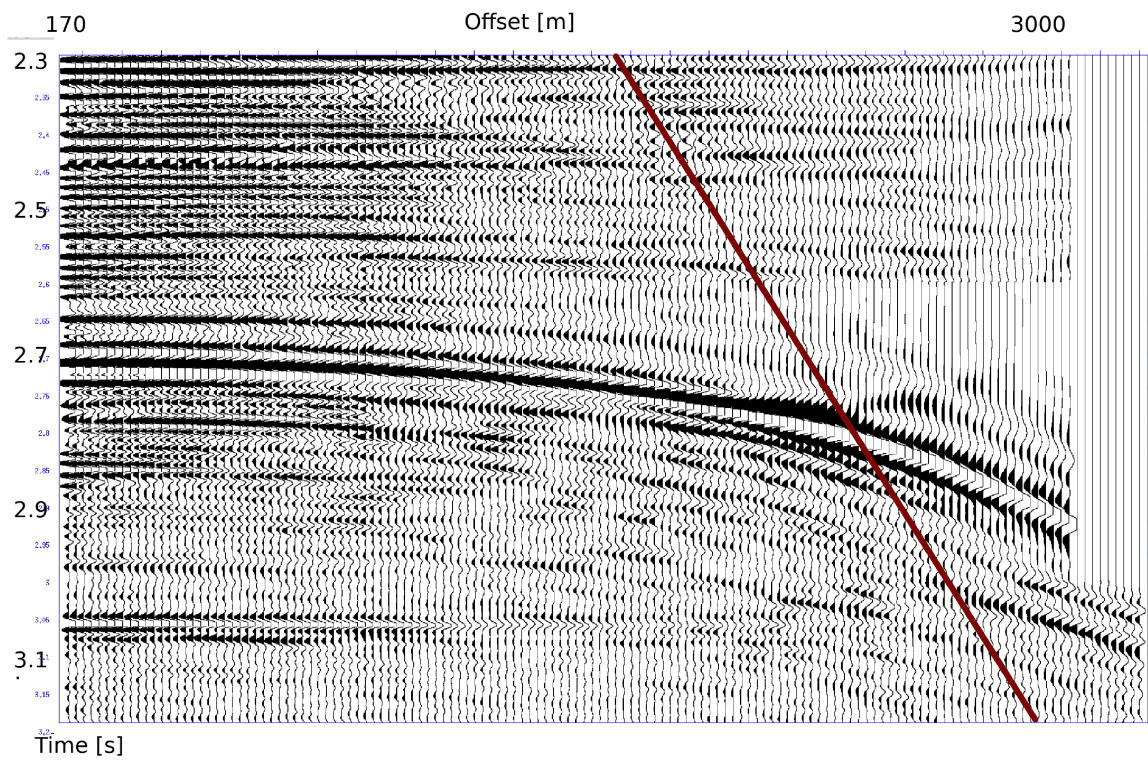


(b) NMO-corrected with velocities from CMP 4280 provided by TGS

Figure 27: Field data of CMP 4300, NMO-corrected with Seismic Unix



(a) NMO-corrected with velocities that were picked at CMP 4300



(b) NMO-corrected with velocities from CMP 4280 provided by TGS

Figure 28: Field data of CMP 4300, NMO-corrected with Seismic Unix, close-up

## 7 Conclusions and Outlook

In this bachelor thesis I developed an alternative way to obtain the normal-moveout-velocities of a CMP using the spectral bandwidth of the the stacked traces.

It is not possible to use the conventional definition of bandwidth as a parameter for good stacking velocities. It is necessary to also take the maximum of the power spectrum or another value corresponding to the amplitude of the signals into account.

At times when different reflections are present the bandwidth-method delivers better results than the semblance, which means that it is possible to focus the correct  $v_{\text{NMO}}$  stronger.

A disadvantage is that this method requires more computational effort than the semblance because it is necessary to explicitly apply the NMO-correction and compute the power spectra before determining the bandwidth.

Another disadvantage is that the computed bandwidth depends on the velocity range that is chosen. It is not possible to identify small signals when there are signals with bigger amplitudes that have their best fitting  $v_{\text{NMO}}$  in the range in which the velocities for the reference spectra are chosen. In this case it is necessary to reduce the velocity range in which the reference spectra are defined or to suppress the multiple reflections.

When picking velocities by hand the adaptation of the velocity range in which the reference spectra are defined can be easily implemented in a program. When automatizing the picking process this might be more difficult.

To automatize the picking process it would be possible to first perform a velocity analysis using the semblance. With the resulting velocity profile it would then be possible to define a range of velocities around this profile for which you apply a bandwidth analysis. Thus the  $v_{\text{NMO}}$  of the multiple reflections are not chosen as reference spectra.

The bandwidth has only a few values that are not zero and these values are almost exclusively aligned around the path of the correct  $v_{\text{NMO}}$ . Therefore a polynomial regression analysis might deliver better results when using the bandwidth instead of the semblance.

It might be helpful to search for a bandwidth-parameter that does not depend on the velocity range in which the bandwidth analysis is applied.

Maybe the correct stacking-velocities are even more delimited if also the frequency shift towards lower frequencies and the semblance are taken into account.

## 8 Acknowledgement

I would like to thank everyone who directly or indirectly contributed to this thesis.

I owe thanks to

- Prof. Dr. Christian Hübscher for helping me to correct the used field data and to verify my results,
- Pavel Znak, Dr. Sergius Dell and Dr. Jan Walda who supported me whenever I had problems with my code,
- Prof. Dr. Dirk Gajewski for helping me to develop the structure of this thesis
- PD Dr. Claudia Vanelle and Rafael Tappe Maestro and Matthias Hartge for proof-reading
- and finally TGS for providing the data.

## 9 References

- [1] Yilmaz,Öz *SEISMIC DATA ANALYSIS*. Society of Exploration Geophysicists, 2001
- [2] Perroud,Hervé et al. *Nonstretch NMO*. GEOPHYSICS, 2004
- [3] Gurgel, Klaus-Werner. *FFT und Fensterfunktionen*. Zeitreihenanalyse Universität Hamburg, 2018
- [4] MathWorks. *FFT for Spectral Analysis*. <https://www.mathworks.com/help/matlab/examples/fft-for-spectral-analysis.html>; date of access: 04.07.2019
- [5] Lohninger, Hans. *Fensterfunktionen in der FFT*. [http://www.statistics4u.info/fundstat\\_germ/ee\\_fft\\_windowing.html](http://www.statistics4u.info/fundstat_germ/ee_fft_windowing.html); date of access: 22.07.2019
- [6] Großmann,Siegfried. *Heisenbergsche Unschärferelation*. [https://www.weltderphysik.de/fileadmin/user\\_upload/Redaktion/Gebiete/theorien/Grundzuege\\_der\\_QM/201011\\_unschaerfe.pdf](https://www.weltderphysik.de/fileadmin/user_upload/Redaktion/Gebiete/theorien/Grundzuege_der_QM/201011_unschaerfe.pdf); date of access: 04.07.2019
- [7] Weiß, Benedikt J. et al. *Model optimization in the presence of complex slat structures using ray-based methods*. NORSAR, 2009
- [8] Vanelle, Claudia. *Personal communication*.
- [9] Walda, Jan. *Personal communication*.

## 10 List of Figures

1	Snellius' Law . . . . .	7
2	CMP-gather . . . . .	8
3	NMO-stretch . . . . .	11
4	FFT without taper window . . . . .	13
5	Taper window . . . . .	14
6	FFT with and without taper window . . . . .	14
7	Heisenberg's uncertainty principle . . . . .	15
8	Slightly wrong stacking-velocity . . . . .	16
9	Very wrong stacking-velocity . . . . .	16
10	Datasets . . . . .	18
11	NMO-corrected synthetic data . . . . .	20
12	NMO-corrected field data . . . . .	21
13	NMO-corrected seafloor reflection . . . . .	22
14	Semblance of seafloor reflection . . . . .	23
15	Power spectra of stacked seafloor reflection . . . . .	24
16	Power spectra of unstacked seafloor reflection . . . . .	25
17	Normalized power spectra of stacked seafloor reflection . . . . .	26
18	Synthetic data stacked with a very wrong velocity . . . . .	26
19	Definition of bandwidth . . . . .	28
20	Bandwidth of seafloor reflection . . . . .	28
21	Semblance and bandwidth of field data . . . . .	30
22	Semblance and bandwidth of field data, close-up . . . . .	31
23	Semblance and improved bandwidth of field data . . . . .	33
24	Semblance and bandwidth for different muting functions . . . . .	34
25	Semblance and bandwidth with picked velocities . . . . .	35
26	Migrated field data, provided by TGS, modified by Ben Schmidt . . . . .	37
27	Field data, NMO-corrected with SU, complete CMP . . . . .	38
28	Field data, NMO-corrected with SU, zoomed . . . . .	39

## 11 Versicherung an Eides statt

Hiermit versichere ich an Eides statt, dass ich die vorliegende Arbeit im Studiengang Bachelor of Science Geophysik/Ozeanographie selbstständig verfasst und keine anderen als die angegebenen Hilfsmittel – insbesondere keine im Quellenverzeichnis nicht benannten Internet-Quellen – benutzt habe. Alle Stellen, die wörtlich oder sinngemäß aus Veröffentlichungen entnommen wurden, sind als solche kenntlich gemacht. Ich versichere weiterhin, dass ich die Arbeit vorher nicht in einem anderen Prüfungsverfahren eingereicht habe und die eingereichte schriftliche Fassung der auf dem elektronischen Speichermedium entspricht. Ich bin mit der Ausstellung der Arbeit in der Fachbibliothek einverstanden.

Hamburg, den

Ben Schmidt